5-10-2008

Ejection of Supermassive Black Holes from Galaxy Cores

Alessia Gualandris

David Merritt

Recommended Citation
Astrophysical Journal 678 (2008) 780-797

DRAFT VERSION FEBRUARY 1, 2008
Preprint typeset using LaTeX style emulateapj v. 10/09/06

EJECTION OF SUPERMASSIVE BLACK HOLES FROM GALAXY CORES

ALESSIA GUALANDRIS AND DAVID MERRITT
Center for Computational Relativity and Gravitation, Rochester Institute of Technology, 78 Lomb Memorial Drive, Rochester, NY 14623
Draft version February 1, 2008

ABSTRACT

Recent numerical relativity simulations have shown that the emission of gravitational waves during the merger of two supermassive black holes (SMBHs) delivers a kick to the final hole, with a magnitude as large as $4000\,\mathrm{km\,s^{-1}}$. We study the motion of SMBHs ejected from galaxy cores by such kicks and the effects on the stellar distribution using high-accuracy direct N-body simulations. Following the kick, the motion of the SMBH exhibits three distinct phases. (1) The SMBH oscillates with decreasing amplitude, losing energy via dynamical friction each time it passes through the core. Chandrasekhar's theory accurately reproduces the motion of the SMBH in this regime if $2 \lesssim \ln\Lambda \lesssim 3$ and if the changing core density is taken into account. (2) When the amplitude of the motion has fallen to roughly the core radius, the SMBH and core begin to exhibit oscillations about their common center of mass. These oscillations decay with a time constant that is at least 10 times longer than would be predicted by naive application of the dynamical friction formula. During this phase, the SMBH is typically displaced from the peak of stellar density by roughly the core radius. (3) Eventually, the SMBH reaches thermal equilibrium with the stars. We use straightforward scaling arguments to estimate the time for the SMBH's oscillations to damp to the Brownian level in real galaxies and infer times as long as $\sim 1\,\mathrm{Gyr}$ in the brightest galaxies. The longevity of the oscillations makes this mechanism competitive with others that have been proposed to explain double or offset nuclei. Ejection of SMBHs also results in a lowered density of stars near the galaxy center; mass deficits as large as five times the SMBH mass are produced for kick velocities near the escape velocity. We compare the N-body density profiles with luminosity profiles of early-type galaxies in Virgo and show that even the largest observed cores can be reproduced by the kicks, without the need to postulate "hypermassive" binary SMBHs. Implications for displaced AGNs and helical radio structures are discussed.
Subject headings: galaxies:nuclei - stellar dynamics

1. INTRODUCTION

The recent breakthroughs in numerical relativity (Pretorius 2005; Campanelli et al. 2006; Baker et al. 2006a) have allowed a number of groups to evolve binary black holes (BHs) to full coalescence. The final inspiral is driven by emission of gravitational waves, and in typical (asymmetric) inspirals, a net impulse is imparted to the system due to anisotropic emission of the waves (Bekenstein 1973; Fitchett & Detweiler 1984; Favata et al. 2004). Early arguments that the magnitude of the recoil velocity would be modest for non-spinning BHs (Redmount & Rees 1989) were confirmed by the simulations, which found $V_{\rm kick} \lesssim 200\,\mathrm{km\,s^{-1}}$ in the absence of spins (Baker et al. 2006b; González et al. 2007b; Herrmann et al. 2007). The situation changed dramatically following the first simulations of "generic" binaries, i.e., binaries in which the individual BHs were spinning and in which the spins were allowed to have arbitrary orientations (Campanelli et al. 2007b). Kicks as large as $\sim 2000\,\mathrm{km\,s^{-1}}$ have now been confirmed (Campanelli et al. 2007a; González et al. 2007a; Tichy & Marronetti 2007), and simple scaling arguments suggest that the maximum kick velocity would probably increase to $\sim 4000\,\mathrm{km\,s^{-1}}$ in the case of maximally-spinning holes (Campanelli et al. 2007a). The most propitious configuration for the kicks consists of an equal-mass binary in which the individual spin vectors are oppositely aligned and oriented parallel to the orbital plane. The kick amplitude also depends sensitively on the angle between the BH spin vectors and their linear momenta shortly before the plunge (Campanelli et al. 2007c).

Electronic address: alessiag,merritt@astro.rit.edu

Galaxy escape velocities are $\lesssim 3000\,\mathrm{km\,s^{-1}}$ (Merritt et al. 2004), which means that gravitational wave recoil can in principle displace coalescing supermassive black holes (SMBHs) arbitrarily far from galaxy centers, or even eject them completely. The actual distribution of kick velocities is very uncertain, since it depends on the unknown distribution of binary mass ratios and spins, but most kicks are probably $\lesssim 10^3\,\mathrm{km\,s^{-1}}$. A SMBH that is kicked with less than escape velocity will travel some maximum distance from the galaxy center after which its orbit decays due to dynamical friction; most of the energy loss takes place during passages through the galaxy center. Removal of the SMBH from the core has the effect of transferring kinetic energy to the stars and lowering the core density (Redmount & Rees 1989; Merritt et al. 2004; Boylan-Kolchin et al. 2004). This implies a more gradual return of the SMBH to a zero-velocity state than in a galaxy with fixed density.

In fact, however, the SMBH is not expected to ever reach a state of zero kinetic energy. When its energy falls to a value

$$\frac{1}{2}M_{\rm BH}V^2 \approx \frac{1}{2}m_\star \mathrm{v}_\star^2 \qquad (1)$$

with respect to the galaxy central potential, where $m_\star$ and $\mathrm{v}_\star$ are a typical stellar mass and velocity respectively, random gravitational perturbations from stars act to accelerate the SMBH as often as they decelerate it. This is the regime of gravitational Brownian motion (Young 1977; Bahcall & Wolf 1976; Merritt et al. 2007). A natural definition of the "return time" of a kicked SMBH is the time required for dynamical friction to reduce the SMBH's mean kinetic energy to the Brownian value. Applying standard expressions for

the dynamical friction force leads one to the conclusion that this would occur in a relatively short time, of order a few orbital periods, after dynamical friction has returned the kicked SMBH to the core.

The *N*-body simulations presented here were designed to test these expectations by evaluating the return times of kicked SMBHs and by quantifying the induced changes in galaxy structure. These processes can not be studied accurately using classical dynamical friction theory since the SMBH substantially modifies the core as it recoils and falls back. Approximate *N*-body schemes, e.g. tree or grid codes, are also not well suited to the problem since they can not robustly follow both the early (collisionless) and late (collisional) evolution of the SMBH. Large particle numbers are required in order to cleanly separate the collisional and collisionless regimes.

These various requirements can currently be met only with parallel, direct *N*-body codes running on special-purpose supercomputers. Our simulations use the ϕGRAPE integrator (Harfst et al. 2007) as implemented on `gravitySimulator`, a 32-node supercomputer employing GRAPE-6A accelerator boards (Fukushige et al. 2005).

Our findings are surprising in one important respect. After returning to the core, the kicked SMBH exhibits long-lived oscillations with amplitude comparable to the core radius[1]. These oscillations eventually decay but with a time constant that is at least an order of magnitude longer than would be predicted by a straightforward application of the dynamical friction equation. We demonstrate that the existence, amplitude and damping time of these oscillations are independent of the number N of "star" particles used in the simulations, for N up to 2×10^6. The oscillations are similar to those first reported by R. Miller and collaborators (Miller & Smith 1992; Miller 1996) in their pioneering *N*-body studies of the central regions of galaxies. A number of other authors have reported low effective values of the dynamical friction force as it acts on massive objects that inspiral into constant-density cores (Bontekoe 1988; Bertin et al. 2003; Read et al. 2006) or on rotating bars (Weinberg & Katz 2002; Valenzuela & Klypin 2003). Our use of a high-accuracy, direct-summation *N*-body code combined with large particle numbers greatly reduces the possibility that our results are an artifact of the potential calculation scheme, an issue that has plagued the interpretation of similar results in the past (Zaritsky & White 1988).

§ 2 describes the initial models and the *N*-body algorithm. Evolution of the SMBH's orbit is described in detail in § 3, and the induced changes in galaxy structure are described in § 4, where the *N*-body models are compared to luminosity profiles of core galaxies. § 5 presents estimates of the SMBH return times in real galaxies, and § 6 discusses some of the observable consequences of the kicks.

2. INITIAL MODELS AND NUMERICAL METHODS

The light profiles of elliptical galaxies and the bulges of spiral galaxies are generally well described in terms of the Sérsic model (Sérsic 1963; Sersic 1968), which is a generalization of the de Vaucouleurs (1948, 1959) law. The most luminous elliptical galaxies depart systematically from the Sérsic law near the center, where they show evidence for partially depleted stellar cores (Faber et al. 1997; Milosavljević et al. 2002; Graham 2004; Ferrarese et al. 2006). Formation of a binary SMBH following a galaxy "major merger" has been shown to produce cores of roughly the right magnitude (Milosavljević & Merritt 2001; Merritt 2006), although some observed cores are too large to be easily explained by this model (a point we return to in detail below).

TABLE 1
PARAMETERS OF THE INITIAL MODELS.

name	n	α	r_b	γ	$M_\mathrm{BH}/M_\mathrm{gal}$
A1	4.0	2.0	0.014	0.55	1.0×10^{-3}
A2	4.0	2.0	0.0095	0.55	1.0×10^{-3}
B	4.0	2.0	0.027	0.55	3.0×10^{-3}

As approximate representations of galaxies with binary-depleted cores, we adopt core-Sérsic models (Graham et al. 2003) for our initial conditions. The *space* density profile of a galaxy that follows the core-Sérsic law in projection can be accurately approximated as (Terzić & Graham 2005)

$$\rho(r)=\rho'\left[1+\left(\frac{r_\mathrm{b}}{r}\right)^\alpha\right]^{\gamma/\alpha}\left[\left(r^\alpha+r_\mathrm{b}^\alpha\right)/R_\mathrm{e}^\alpha\right]^{-p/\alpha}e^{-b\left[\left(r^\alpha+r_\mathrm{b}^\alpha\right)/R_\mathrm{e}^\alpha\right]^{1/n\alpha}} \quad (2)$$

with

$$\rho' = \rho_\mathrm{b}\,2^{(p-\gamma)/\alpha}\left(\frac{r_\mathrm{b}}{R_\mathrm{e}}\right)^p e^{b\left(2^{1/\alpha}r_\mathrm{b}/R_\mathrm{e}\right)^{1/n}}. \quad (3)$$

Equation (2) is a modification of the Prugniel-Simien model (Prugniel & Simien 1997). Here, R_e is the effective (half-mass) radius of the projected galaxy; r_b is the break (core) radius; ρ_b is the space density at $r=r_b$; and α regulates the sharpness of the transition from core to outer profile. The parameter n describes the curvature of the Sérsic profile and b and p are fixed functions of n (Prugniel & Simien 1997; Terzić & Graham 2005). Monte-Carlo initial conditions were generated using the scheme of Szell et al. (2005), after including the gravitational potential of a central point particle representing the SMBH.

The parameters used for our initial models are listed in Table 1. The table also reports names for the different runs based on the adopted ratio of SMBH mass to galaxy mass and initial core radius. Core radii were chosen so as to give initial mass deficits of roughly M_BH, as observed for the majority of luminous early-type galaxies (Merritt 2006). We note that $\gamma=0.5$ is the shallowest power-law profile that is consistent with a non-negative, isotropic distribution of stellar velocities around the BH.

The initial models were evolved using the ϕGRAPE numerical integrator (Harfst et al. 2007). This direct-summation code employs a fourth-order Hermite integrator with predictor-corrector scheme and hierarchical time steps. The MPI parallelization strategy is designed to minimize the amount of communication among different computing nodes and to make efficient use of the special-purpose GRAPE hardware. All the simulations presented in this work were performed on the 32-node cluster `gravitySimulator`[2] at the Rochester Institute of Technology. Most of our simulations used $N=0.5\times10^6$ equal-mass particles to represent the galaxy although some runs used larger N. We set the ratio of BH mass to galaxy mass, $M_\mathrm{BH}/M_\mathrm{gal}$, to be $(1,3)\times10^{-3}$, typical for observed galaxies (Merritt & Ferrarese 2001). For each model described in Table 1, we chose eleven different values of the kick velocity V_kick in units of the central escape

[1] A movie showing the oscillations is available at http://ccrg.rit.edu/Research/Publications.php?paper=0708.0771.

[2] http://wiki.cs.rit.edu/bin/view/GRAPEcluster

speed $V_{\rm esc}$: $V_{\rm kick} = (0.1, 0.2, .., 1.1) \times V_{\rm esc}$; the latter was computed numerically from the initial N-body models. In order to guarantee energy conservation, we used a time-step accuracy parameter $\eta = 0.01$. This ensures a relative energy error smaller than one part in 10^6. An accuracy parameter twice as big would approximately halve the integration time but would result in a relative energy error of 10^{-4}, which we do not consider acceptable for this study. A softening length $\epsilon = 10^{-4}$ was assigned to both the stars and the BH. Such a small softening length has been shown not to affect even the Brownian motion of a massive particle in models like ours (Merritt et al. 2007).

Throughout the paper we adopt units according to which the gravitational constant G, the effective radius $R_{\rm e}$ in equation (2), and the total galaxy mass $M_{\rm gal}$ are unity. The models can be scaled to physical units as follows:

$$[T] = \left(\frac{GM_{\rm gal}}{R_{\rm e}^3}\right)^{-1/2} \tag{4}$$

$$= 7.75\times10^6 {\rm yr}\left(\frac{M_{\rm gal}}{10^{11}\,{\rm M}_\odot}\right)^{-1/2}\left(\frac{R_{\rm e}}{3\,{\rm kpc}}\right)^{3/2}, \tag{5}$$

$$[V] = \left(\frac{GM_{\rm gal}}{R_{\rm e}}\right)^{1/2} \tag{6}$$

$$= 378\,{\rm km\,s^{-1}}\left(\frac{M_{\rm gal}}{10^{11}\,{\rm M}_\odot}\right)^{1/2}\left(\frac{R_{\rm e}}{3\,{\rm kpc}}\right)^{-1/2}. \tag{7}$$

3. THE BLACK HOLE MOTION

3.1. *General Remarks*

Figure 1 (which can be compared with Fig. 1 of Madau & Quataert 2004 shows BH trajectories in models A1, A2 and B for $V_{\rm kick}/V_{\rm esc} = (0.4, 0.7, 0.9, 1.1)$. For $V_{\rm kick} \geq V_{\rm esc}$ the black hole escapes the galaxy on an unbound orbit. The maximum displacement of the BH ($r_{\rm max}$) is shown in Figure 2. The data from the simulations (points) are compared to theoretical (dotted lines) and numerical (dashed lines) estimates of $r_{\rm max}$ in the absence of dynamical friction. The theoretical and numerical estimates are obtained from the initial N-body data by assuming conservation of total energy for the BH: $r_{\rm max}$ is the distance at which the gravitational potential of the system equals the initial total energy of the BH. For the theoretical solution we use the expression of the potential in a core-Sérsic model (see equations 7 through 13 of Terzić & Graham 2005) while for the numerical solution we compute the potential at different radii from the N-body data. The two estimates are for practical purposes indistinguishable.

Dynamical friction affects the maximum displacement of the BH only for moderately large kicks, where the data points appear systematically lower than the theoretical curves. Values of $r_{\rm max}$ larger than the expected turning points in the first orbit are due to the rapidly-expanding core.

During the initial outward journey, dynamical friction does not strongly influence the motion of the BH, and the maximum displacement is similar to that of an energy-conserving orbit. We note that a kick velocity larger than about $0.3V_{\rm esc}$ is necessary to bring the BH beyond the core. Due to the combined effect of the kick and dynamical friction, the BH displays a damped oscillatory motion. The number of radial oscillations increases with $V_{\rm kick}$; for $V_{\rm kick} = 0.9V_{\rm esc}$ the BH experiences ~ 5 full radial oscillations before returning to the core. Almost all of the energy loss to dynamical friction takes

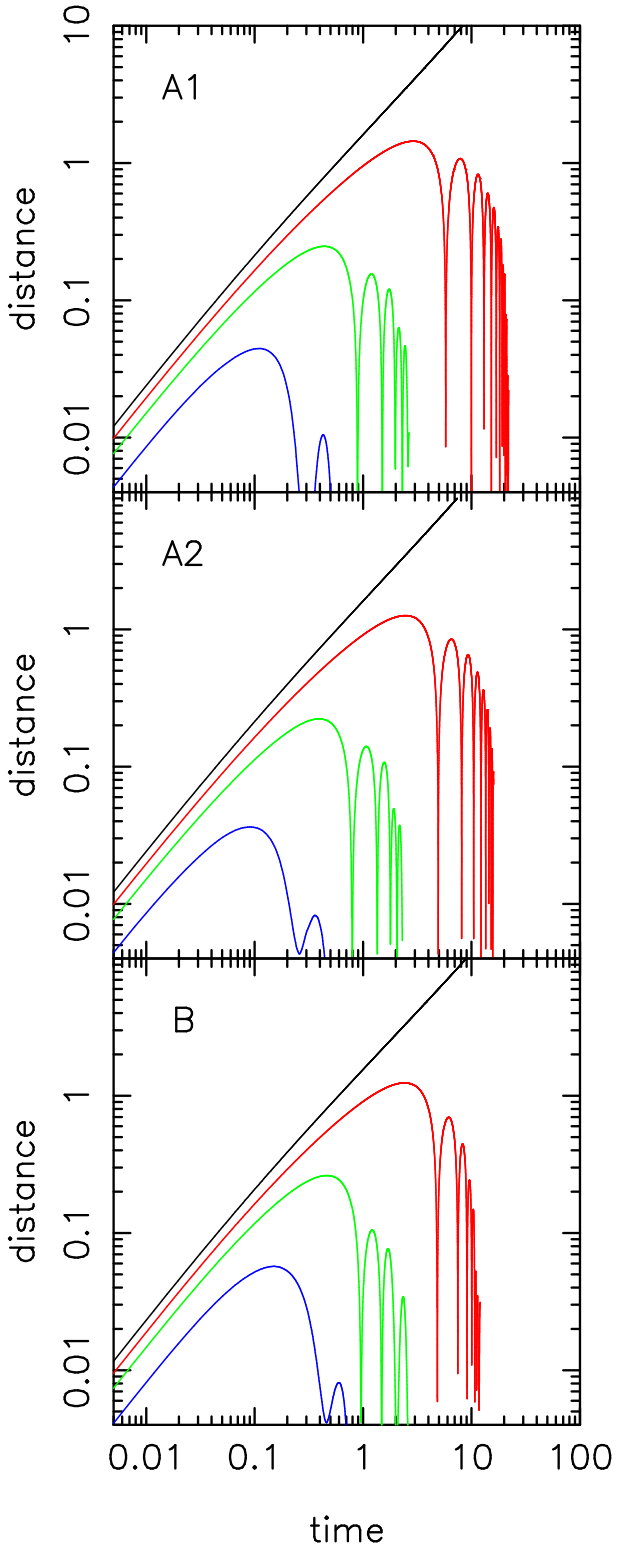

FIG. 1.— BH trajectories in models A1, A2 and B, for $V_{\rm kick}/V_{\rm esc} = 0.4$ (blue/lower), 0.7 (green), 0.9 (red) and 1.1 (black).

place during the short intervals that the BH passes through the core. This is shown in Figure 3 which plots the evolution of the BH specific energy E in Model A1 with $V_{\rm kick} = 0.9V_{\rm esc}$, where

$$E \equiv \frac{V^2}{2} - \sum_{i=2}^{N} \frac{m_i}{\sqrt{(\mathbf{x}_i - \mathbf{X})^2 + \epsilon^2}} \tag{8}$$

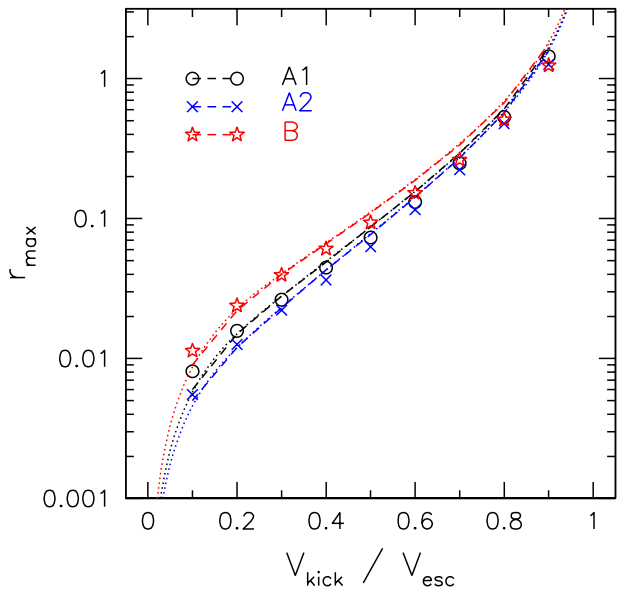

FIG. 2.— Maximum displacement of the BH from the galaxy center. The data points show the results from the simulations while the lines are estimates in the absence of dynamical friction. The dashed lines represent numerical estimates from the computation of the potential of the N-body system at time $t = 0$ while the dotted lines represent theoretical estimates from the analytic expression of the potential in a core-Sérsic model.

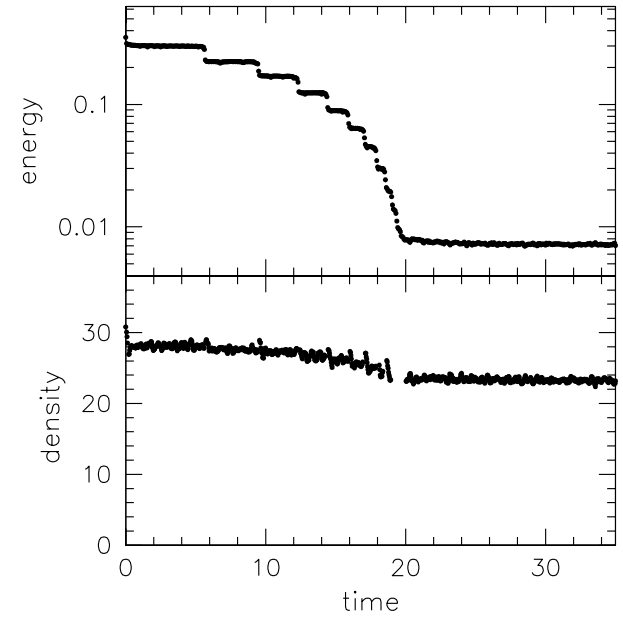

FIG. 3.— *Upper panel:* Specific energy of the BH particle versus time in Model A1 with $V_{\rm kick} = 0.9V_{\rm esc}$. Almost all of the energy loss occurs during passages through the core. *Lower panel:* Mean density in a sphere of radius 0.05 centered on the point of maximum density in the core of the galaxy (excluding the BH).

and the summation is over the "star" particles[3]. The energy lost during the initial emergence from the core appears to be less than during subsequent passages, suggesting that dynamical friction requires a finite time to "turn on" after the kick. During the first few oscillations, the BH's motion remains essentially rectilinear, but eventually the Y- and Z-components of the motion become important due to non-sphericities in the galaxy potential and also to perturbations from stars. At late times, the BH's motion is essentially random, similar to that of a Brownian particle in a fluid. Figure 3 also shows the mean density in a sphere of fixed radius whose center is located at the estimated density peak (computed via the algorithm described in § 3.2). The core density decreases rapidly following the initial ejection, then more gradually as the BH returns again and again to the core, losing energy to the stars each time.

[3] Unless otherwise noted, upper-case variables X and V refer to the BH particle while lower-case symbols are reserved for the star particles.

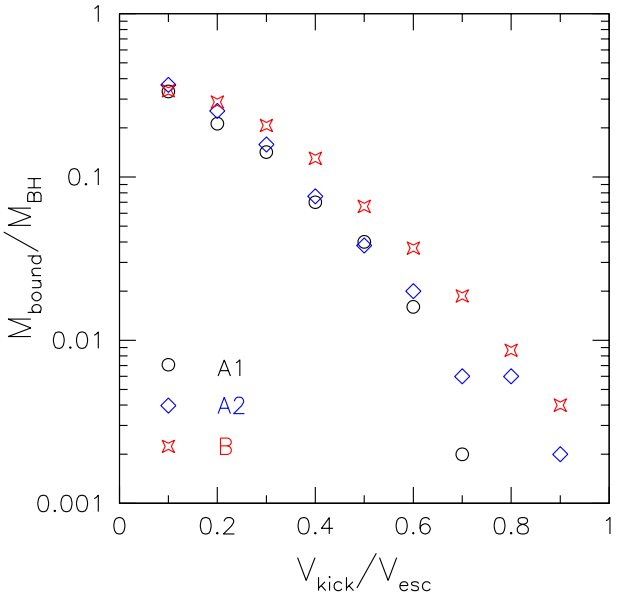

FIG. 4.— Stellar mass bound to the BH in the initial models.

Figure 4 shows the mass in stars bound to the BH at $t = 0$. The bound mass was computed by counting all the stars, within the influence radius r_h, which formed a bound two-body system with the BH particle. The influence radius was defined as the radius containing a mass in stars equal to twice $M_{\rm BH}$. The bound mass decreases steeply with $V_{\rm kick}$, as noted in earlier studies (Merritt et al. 2004; Boylan-Kolchin et al. 2004), and is ignorable for $V_{\rm kick} \gtrsim 0.6V_{\rm esc}$.

In all cases where the kick velocity was large enough to remove the BH completely from the core (i.e. $V_{\rm kick} \gtrsim 0.3V_{\rm esc}$), we observed three distinct regimes of the motion. In Phase I, the BH's motion is well predicted by Chandrasekhar's dynamical friction theory, after taking into account the changing size of the galaxy core where most of the friction occurs. This is the phase illustrated in Figure 1; in Figure 3, Phase I extends until $t \approx 20$. Phase II begins roughly when the amplitude of the BH's motion had decayed to the size of the core. In this phase, the energy of the BH's orbit continues to decay but with a much longer time constant than predicted by Chandrasekhar's formula. The BH and the core oscillate about their common center of mass in this regime. In Phase III, the BH's energy has dropped to the thermal level. Phase II is generally longer than Phase I, and this would presumably be even more true in real galaxies since the amplitude of thermal oscillations is much lower than in our simulations implying a longer

time to reach the Brownian regime. We discuss these three regimes in detail below.

3.2. *Phase I*

The extent of Phase I is clearly indicated in the plots of BH energy vs. time (e.g. Fig. 3): a distinct "knee" appears in the $E(t)$ curves marking the end of this phase. Values of T_I, the elapsed time from the kick until the end of Phase I, are given in Table 2.

We compared the evolution of the BH's motion in Phase I with the predictions of Chandrasekhar's dynamical friction theory (Chandrasekhar 1943). Such comparisons are problematic since much of the energy exchange between BH and stars occurs during passages through the galaxy's core, and the core density changes significantly with time due to the BH's motion. We dealt with this problem by breaking the BH's motion into segments, each containing one passage through the center, and assuming that the galaxy's density remained constant during each segment.

Chandrasekhar (1943) derived his expression for the dynamical friction acceleration $F_{\rm df}$ assuming an infinite, homogeneous and unchanging background of perturbers (stars). In the limit that the mass of the heavy object greatly exceeds the masses of the stars, the acceleration is predicted to be

$$F_{\rm df} \approx -2\pi G^2 \rho M_{\rm BH} \ln(1+\Lambda^2) V^{-2} N(<V,r), \qquad (9)$$

where $\rho(\mathbf{r})$ is the mass density of stars at the BH's position, $(1/2)\ln(1+\Lambda^2)$ is the Coulomb logarithm, V is the BH's instantaneous velocity, and $N(<V,\mathbf{r})$ is the fraction of stars at $\mathbf{r}$ that are moving (in the frame of the galaxy) with velocities less than V.

Some care must be taken in the definition of the Coulomb logarithm. One commonly writes

$$\ln\left(1+\Lambda^2\right) \approx 2\ln\Lambda \approx 2\ln(p_{\rm max}/p_{\rm min}) \qquad (10)$$

where $p_{\rm min}$ and $p_{\rm max}$ are the minimum and maximum effective impact parameters of the stars that contribute to the frictional force, and $p_{\rm max} \gg p_{\rm min}$. However, $p_{\rm min}$ depends on the field-star velocity (White 1949; Merritt 2001) and $p_{\rm max}$ is likewise ill-defined since a realistic stellar system is inhomogeneous and has no outer boundary.

Numerous N-body simulations have been carried out to evaluate Chandrasekhar's formula in the case of a massive particle inspiraling toward the center of a galaxy (White 1983; Bontekoe & van Albada 1987; Bontekoe 1988; Weinberg 1989; Cora et al. 1997; Bertin et al. 2003). Early work was typically based on approximate N-body schemes and the results were often discrepant from study to study (Zaritsky & White 1988). These differences appear to have been resolved in the last few years through the use of direct-summation codes (Spinnato et al. 2003; Merritt 2006), which consistently find $4 \lesssim \ln\Lambda \lesssim 6$ for inspiral of massive point particles, on circular or near-circular orbits, into the centers of galaxies with steeply-rising density profiles. Fewer experiments have been done with highly eccentric orbits, although Just & Peñarrubia (2005), using an approximate method, find $2 \lesssim \ln\Lambda \lesssim 3$ for orbits with moderate eccentricities.

In general, we expect the effective value of $\ln\Lambda$ to be smaller for radial orbits than for circular motion. The dynamical friction force arises from a polarization of the stellar density which produces an over-dense region, or wake, behind the massive object (Mulder 1983). A finite time, of order a galaxy crossing time, is presumably required for this wake to be set up. In the case of a gradually-decaying circular orbit, the galaxy is able to reach a quasi-steady state after a few orbits of the massive object. In our case, the position and velocity of the BH are changing dramatically over one crossing time, so that the wake never has a chance to establish its steady-state amplitude; indeed just after apocenter passages, the over-dense region can be seen to lie in *front* of the BH.

In order to determine the effective value of $\ln\Lambda$ in the N-body integrations, we computed BH trajectories using Chandrasekhar's formula (equation 9) with various values of the $\ln\left(1+\Lambda^2\right)$ term (henceforth written simply as $2\ln\Lambda$) and compared them with the N-body trajectories. The following procedure was followed.

1. The density center of the galaxy moves slightly with respect to the origin of the coordinates due to transfer of momentum from the kicked BH to the galaxy. In order to accurately determine the distance of the BH from the galaxy center as a function of time, we recorded full snapshots of the particle positions at frequent intervals, then used the Casertano-Hut (1985) algorithm to find the density center of the stars in each snapshot. A smoothing spline was fit through the measured positions to give a continuous estimate of the center displacement as a function of time, and this displacement was subtracted from the BH positions. (The instantaneous velocity of the density center was ignored, which is a good approximation at least until the end of Phase I.) The resulting correction was at most ~ 0.02; at late times the displacement reached a constant value since the center-of-mass velocity of the system was zero by construction.

2. In order to apply Chandrasekhar's formula we needed to specify the galaxy model. The galaxy's mass distribution changes with time due to the BH's motion; most of this change takes place in the core just after the BH passes through. We therefore fixed all the parameters in equation (2) except for the core radius r_b. We determined the effective value of r_b at the discrete times when the BH passed through the galaxy center by assuming a flat core ($\gamma = 0$) and finding the value of r_b such that the mass contained within r_b according to equation (2), with $\alpha = 2$, was the same as the mass in the N-body model in a sphere of radius r_b centered on the BH. This procedure was always found to yield a unique r_b and accurately recovered the known value of r_b in the initial models.

3. BH trajectories were then computed in a piecewise fashion using Chandrasekhar's formula, starting from one extremum in the BH displacement and continuing until the next extremum, using the value of r_b corresponding to the central passage lying between the two extrema. This was repeated for several values of $\ln\Lambda$. We used equation (5) of Szell et al. (2005) to compute $N(<V,r)$ in equation (9) from the assumed $\rho(r)$.

Figure 5 shows the results for Model A1 with $V_{\rm kick}/V_{\rm esc} = 0.7$ and Model B with $V_{\rm kick}/V_{\rm esc} = 0.8$. During each inward leg of the trajectory, the dynamical friction force hardly affects the motion; only when passing through the dense center is the motion significantly non-ballistic. (This could be seen already in Figures 2 and 3.) The best-fit value of $\ln\Lambda$ was found to lie in the range $2 \lesssim \ln\Lambda \lesssim 3$, and for such values, Chandrasekhar's formula did a good job of reproducing the motion. We found no evidence of a systematic change in the effective value of $\ln\Lambda$ from one time interval to the next.

3.3. *Phase III*

The BH trajectories in Figure 5 are displayed until the amplitude of the oscillations has decayed down to roughly the

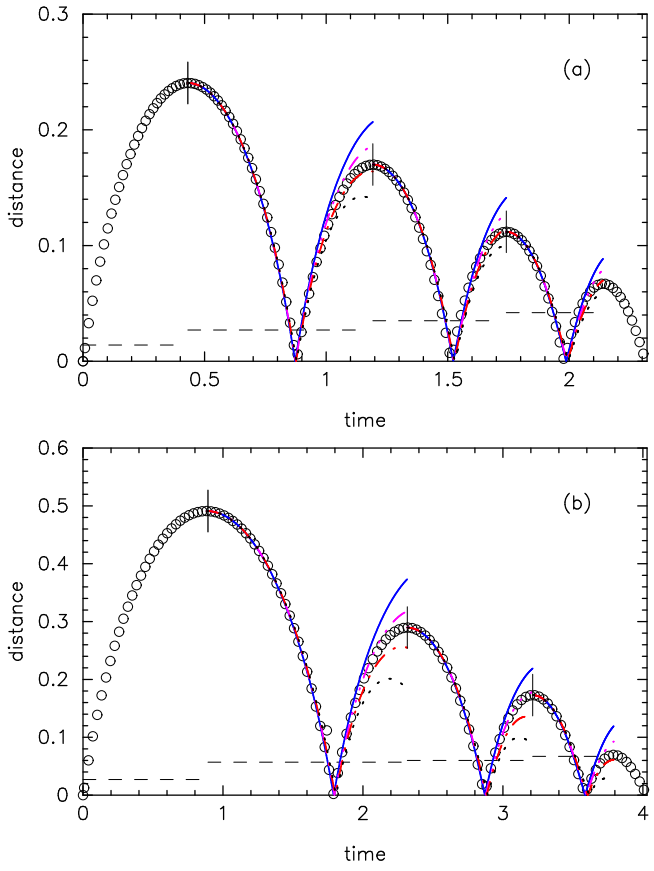

FIG. 5.— Comparison between BH trajectories computed via the N-body integrations (open circles) and via Chandrasekhar's formula (9) (lines). The N-body models were A1 ($M_{\rm BH} = 0.001$) with $V_{\rm kick} = 0.7V_{\rm esc}$ (a) and B ($M_{\rm BH} = 0.003$) with $V_{\rm kick} = 0.8V_{\rm esc}$ (b). Theoretical trajectories were computed in a piecewise manner, starting from extrema in the BH's trajectory (vertical solid lines) and continuing until the next extremum; the core radius r_b of the galaxy model was adjusted as described in the text to give the same core density as in the N-body model at the time when the BH passed through the center. Horizontal dashed lines show the adopted values of r_b. Line colors/styles correspond to different values of $\ln\Lambda$: 1 (blue/solid), 2 (magenta/dashed), 3 (red/dash-dotted), 4 (black/dotted).

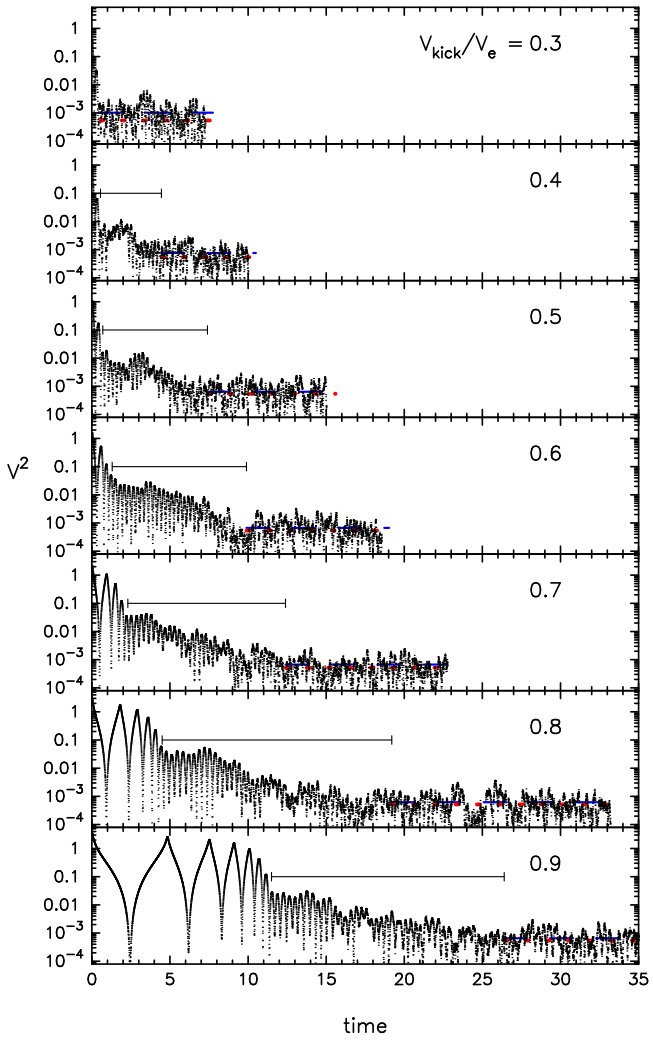

FIG. 6.— Squared BH velocity in seven N-body integrations of Model B. For $V_{\rm kick} \gtrsim 0.4V_{\rm esc}$ the BH moves completely out of the core before falling back. Ticked, horizontal lines demarcate Phase II. Blue (dashed) lines show $\langle V^2\rangle$ during Phase III, and red (dotted) lines show the mean square velocity predicted by equation (11), which assumes that the BH particle has reached thermal equilibrium with the stars in its vicinity.

core radius. As discussed above, the BH's motion is well predicted by Chandrasekhar's dynamical friction formula in this regime. Shortly after returning to the core, however, the BH's motion was found to depart strikingly from the predictions of Chandrasekhar's formula. A detailed discussion of the motion in "Phase II" is presented below. Before doing so, we consider the motion of the BH at still later times, "Phase III," when it has reached thermal equilibrium with the stars.

Figure 6 shows the squared velocity of the BH, $V^2 = V_x^2 + V_y^2 + V_z^2$, over the full integration interval, for kick velocities $V_{\rm kick} \geq 0.3V_{\rm esc}$ in Model B. For $V_{\rm kick} \gtrsim 0.4V_{\rm esc}$ the BH moves substantially beyond the core during its first oscillation (Fig. 2). At late times, the motion of the BH in each of these integrations appears to be stochastic (i.e. non-quasi-periodic) but with roughly constant amplitude.

The dashed (blue) lines in this figure show $\langle V^2\rangle$, the mean square velocity of the BH averaged over Phase III. (The precise definition of the start of Phase III is given below.) Also shown (dotted red lines) are estimates of the expected value of $\langle V^2\rangle$ for the BH once it reaches statistical equilibrium with the stars. The latter velocity, $V^2_{\rm Brown}$, was computed using

$$V^2_{\rm Brown} = 3\frac{m_\star}{M_{\rm BH}}\tilde{\sigma}^2. \qquad (11)$$

Equation (11) equates the kinetic energy of the BH with the mean kinetic energy of a single star in the core. The quantity $\tilde{\sigma}$ is defined as the 1D velocity dispersion of stars within a sphere of radius $K \times r_h$ centered on the BH, with r_h the BH's influence radius (the radius containing a mass in stars equal to twice $M_{\rm BH}$) and K a constant of order unity. Merritt et al. (2007) used N-body simulations to evaluate K for massive particles at the centers of galaxies with power-law nuclear density profiles, $\rho \sim r^{-\gamma}$. They found that K increases slowly with decreasing γ, to $K \approx 0.8$ when $\gamma = 0.5$. We set $K = 1$ when computing $V_{\rm Brown}$ in Figure 6; the agreement with the measured values is quite good, confirming that the BH behaves as a Brownian particle in Phase III.

Figure 7 shows the rms amplitude of the BH's motion averaged over Phase III. Since the density center of the galaxy drifts, as described above, smoothing splines were first fit to the $\mathbf{X}(t)$ values for the BH and the rms deviations were computed with respect to the smoothed trajectories. Figure 7 shows a general trend of increasing $R_{\rm rms}$ with decreasing core density, as expected if the motion in this regime obeys the

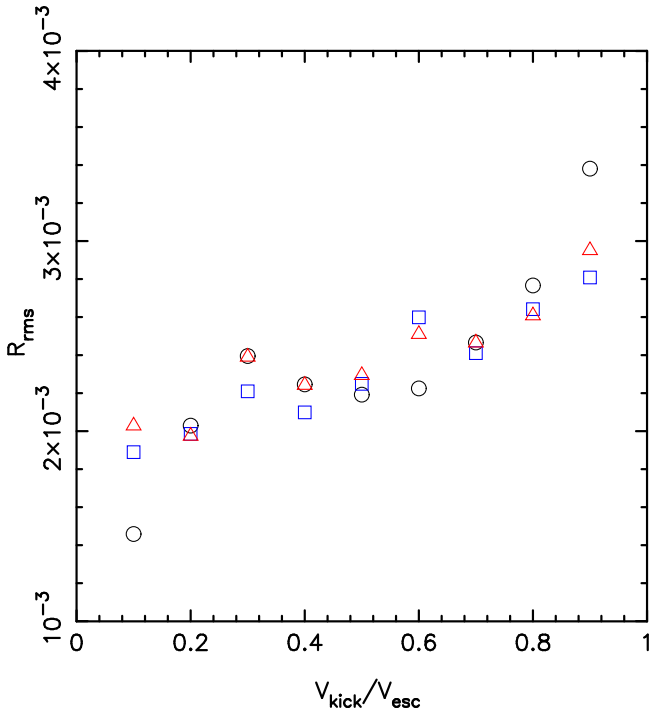

FIG. 7.— RMS amplitude of the BH oscillations in the Brownian regime, Phase III, for models A1 (black/circles), A2 (blue/squares) and B (red/triangles).

virial theorem,

$$\langle V^2\rangle \approx \frac{4}{3}\pi G\rho_c\langle R^2\rangle. \quad (12)$$

This relation (cf. Bahcall & Wolf 1976) assumes a constant-density core, ignores the back-reaction of the BH's motion on the stars, and ignores any coupling between random gravitational perturbations from the stars and the quasi-periodic motion of the BH in the smooth potential of the core. Nevertheless, equation (12) was found to reproduce the measured $R_{\rm rms}$ values in Figure 7 quite well if ρ_c was defined as the mean density of stars within r_h. Fluctuations in $R_{\rm rms}$ about the mean relation in Figure 7 appear to be due primarily to fluctuations in $V_{\rm rms}$ and would presumably be smaller if the $R_{\rm rms}$ values were averaged over longer time intervals. The near agreement between the $R_{\rm rms}$ values for the runs with small and large $M_{\rm BH}$ is a consequence of the larger core size / lower core density in runs with larger $M_{\rm BH}$, which compensates for the lower $\langle V^2\rangle \propto M_{\rm BH}^{-1}$.

We note here that the amplitude of the BH's Brownian motion is always a factor 10 or more smaller than the final core radii of the models (Table 3). This implies that the motion of the BH when it first returns to the core – at the start of Phase II – should not be appreciably affected by discreteness effects, i.e. by perturbations from individual stars. This conclusion is confirmed below.

We note also that the amplitude of Brownian oscillations of BHs in real galaxies (expressed as a fraction of the galaxy effective radius, say) would be smaller than in our models by the factor $\sim\sqrt{(M_{\rm gal}/m_\star)/N}$, i.e. ~ 50 for $M_{\rm gal}=10^9M_\odot$ and ~ 500 for $M_{\rm gal}=10^{11}M_\odot$. The time required for a BH to reach these lower kinetic energies would also presumably be longer than in our simulations, as discussed in more detail below.

3.4. *Phase II*

As noted above, the motion of the BH after returning to the core, and before reaching the Brownian regime, is not well described by Chandrasekhar's formula. Here we consider the motion in this regime ("Phase II").

Figure 6 reveals the following qualitative features.

1. The motion in Phase II is essentially oscillatory, with a period similar to that at the end of Phase I, i.e. roughly equal to the period of oscillation of a test particle moving in the stellar core.

2. There is evidence of additional frequencies affecting the BH's motion. For instance, the amplitude of the oscillations sometimes appears to *increase* temporarily over several periods in a manner suggestive of beats.

3. Averaged over many periods, the mean amplitude of the oscillations decays, but with a time constant that is much longer than observed toward the end of Phase I.

4. Near the end of Phase II, the motion becomes increasingly stochastic, presumably due to perturbations from individual stars. Eventually the BH rms velocity falls to the Brownian (thermal) level marking the start of Phase III.

5. Phase II always begins roughly when the stellar mass interior to the BH's orbit is equal to $M_{\rm BH}$. When $V_{\rm kick}\lesssim 0.3V_{\rm esc}$, the BH never escapes the core, and its motion appears to transition directly from Phase I to Phase III.

Based on Figure 6, the elapsed time in Phase II can be substantially longer than the time spent in Phase I. Understanding the character of the motion in this regime is therefore crucial for predicting the expected displacement of a supermassive BH in a real galaxy following a kick.

We begin by considering a simple model for damped oscillations of a massive particle in a constant-density core. While this model will fail to quantitatively reproduce the motion in Phase II, it provides a useful framework for discussing what is observed in the simulations.

In the absence of dynamical friction, and neglecting the influence of the massive particle's presence on core structure, the motion of the massive particle is simple harmonic oscillation with frequency $\omega_c=\sqrt{(4\pi/3)G\rho_c}$; ρ_c is the core density, assumed constant within a radius r_c. To this motion we add the acceleration due to dynamical friction. If the velocity distribution of the stars that produce the friction is Maxwellian with 1D velocity dispersion σ_c, and if the BH's velocity satisfies $V\ll\sigma_c$, the resulting equation of motion in any coordinate x_i is

$$\ddot{X}_i + T_{\rm df}^{-1}\dot{X}_i + \omega_c^2 X_i = 0 \quad (13)$$

where

$$T_{\rm df} = \frac{3}{8}\sqrt{\frac{2}{\pi}}\frac{\sigma_c^3}{G^2\rho_c M_{\rm BH}\ln\Lambda} \quad (14)$$

is the dynamical friction damping time (Merritt 1985). The condition for underdamped oscillations is $2\omega_c T_{\rm df}>1$, where

$$2\omega_c T_{\rm df} = \frac{\sqrt{6}}{2}\frac{\sigma_c^3}{G^{3/2}\rho_c^{1/2}M_{\rm BH}\ln\Lambda} \quad (15)$$

$$= \frac{\sqrt{6\pi}}{9}F^3\frac{M_c}{M_{\rm BH}\ln\Lambda}, \quad (16)$$

with $M_c\equiv(4/3)\pi\rho_c r_c^3$ the core mass; the second relation uses the "core-fitting" formula of Rood et al. (1972),

$$\sigma_c^2 = F^2\frac{4\pi}{9}G\rho_c r_c^2. \quad (17)$$

$F\approx 2$ for our models. Thus

$$2\omega_c T_{\rm df}\approx 4\frac{M_c}{M_{\rm BH}\ln\Lambda} \quad (18)$$

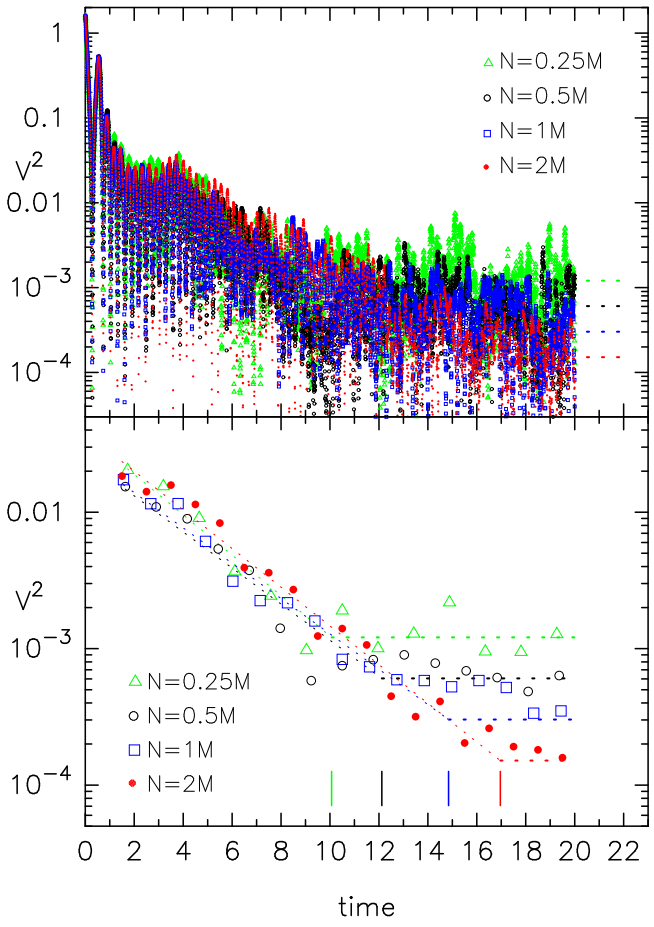

FIG. 8.— Evolution of the BH kinetic energy in a series of integrations of model B with various N, and $V_{\rm kick} = 0.6V_{\rm esc}$. *Top panel:* Squared velocity of the BH versus time. Dashed lines at the right show the predicted values of V^2 in the Brownian regime (eq. 11). *Bottom panel:* Binned values of V^2 in Phases II and III. Dotted lines are least-squares fits to the binned data. These fits are plotted until the time at which they intersect the Brownian V^2; these times are marked by the vertical solid lines. The latter are found to be spaced with roughly constant separation indicating that the time required for the BH to reach thermal equilibrium with the stars increases roughly as $\ln N$.

In our simulations (and in real galaxies), the right hand side of this expression is $\gtrsim 1$, since core masses are $\sim$ a few $M_{\rm BH}$ (Merritt 2006) and $2 \lesssim \ln\Lambda \lesssim 3$ (§ 3.2). It follows that the motion of the BH should be under-damped, though not far from critically damped, after it re-enters the core. The solutions to equation (13) in the under-damped regime are

$$X_i(t) = A_i\, e^{-t/2T_{\rm df}} \sin(\omega_c t + \phi_i)\,. \qquad (19)$$

Writing $\Theta \equiv 2\omega_c T_{\rm df} \gtrsim 1$ and $T_c \equiv 2\pi/\omega_c$, the energy decay time is predicted to be $T_{\rm df} = (\Theta/4\pi)T_c$, i.e. shorter than the orbital period. Such short decay times are in fact observed near the end of Phase I (Figure 5).

However, Figure 6 shows that this is not the case in Phase II: the mean damping time is substantially longer than an orbital period. The abrupt decrease in the energy dissipation rate at the start of Phase II can also be seen in Figure 3(a).

A possible explanation for the slower damping in Phase II is discreteness effects: perturbations from individual stars, some of which act to accelerate the BH, become increasingly competitive with mean-field effects (including dynamical friction) as the BH moves more slowly. Indeed, in the Brownian regime (Phase III), the accelerating perturbations are equally as strong, in a time-averaged sense, as dynamical friction. While the amplitude of the BH oscillations at the onset of Phase II is always much greater than the Brownian amplitude in these simulations (cf. Fig. 7 and the accompanying discussion), it is still conceivable that discreteness effects are responsible for the anomalously slow decay of the BH's orbit at this time.

To securely rule out this possibility, we repeated the integration of model B with $V_{\rm kick} = 0.6V_{\rm esc}$, increasing N up to $N = 2\times10^6$. Figure 8 shows the results. The slowly-damped oscillations in Phase II are clearly not an artifact of a too-small N. In all cases, for instance, the fifth extremum in V^2 (which occurs at $t \approx 1.42$) is comparable or greater in amplitude to the fourth extremum (at $t \approx 1.16$), rather than being much lower in amplitude as would be expected from the above analysis or from Figure 5. We also carried out a number of tests varying the integration time-step parameter η; again, no systematic dependence of the evolution in Phase II on this parameter was observed.

Particularly striking in Figure 8 is the accurately exponential decay of the BH's kinetic energy throughout Phase II; this is clearest in the simulation with largest N, where the exponential damping continues over two decades in energy. We note again that an exponentially decaying energy is predicted by the simple model just presented, but the model predicts a much shorter time constant than what is observed in the N-body simulations.

Figure 9 suggests why Chandrasekhar's (1943) formula might break down in Phase II. The approximation of a stationary galaxy is strongly violated in this regime. The galaxy's density center oscillates with opposite phase to the BH, and with roughly the same frequency and amplitude. This is consistent with the observation that Phase II always begins roughly when the mass in stars inside the BH's orbit is similar to $M_{\rm BH}$. Evidently, in this regime, the BH and the core oscillate about their common center of mass as a two-body system. Chandrasekhar's derivation, which assumed a body on a linear trajectory through an infinite homogeneous medium, is unlikely to apply to oscillations like those in Figure 9, since the BH is periodically accelerated, then decelerated, by the density peak. The rate at which such oscillations decay is known to be sensitively dependent on resonant interactions (Tremaine & Weinberg 1984) and can be arbitrarily low (Louis & Gerhard 1988; Sridhar 1989; Sridhar & Nityananda 1989; Mineau et al. 1990), although we are not aware of any theoretical treatment that is directly applicable to oscillations like those in Figure 9.

Ours is not the first N-body study to observe persistent oscillations of massive objects at the centers of N-body models. Miller & Smith (1992) and Miller (1996) reported a series of N-body integrations, using a grid-based code, of a disk at the center of an axisymmetric galaxy model. They observed what appeared to be over-stable oscillations of particles initially at rest near the center of the disk; the oscillation frequency was roughly $\sqrt{(4\pi/3)G\rho_c}$ and the maximum amplitude was roughly the size of the core. All of these features are characteristic of the oscillations that we observe in Phase II. Miller & Smith (1992) also reported "a couple of experiments in which a massive object was put into orbit within a galaxy model," presumably near the center, and observed "residual oscillations" with amplitude roughly equal to the radius at which the enclosed mass was equal to the object's mass, again similar to what we observe. Miller & Smith (1992) briefly describe a model for the oscillations, in which periodic motion

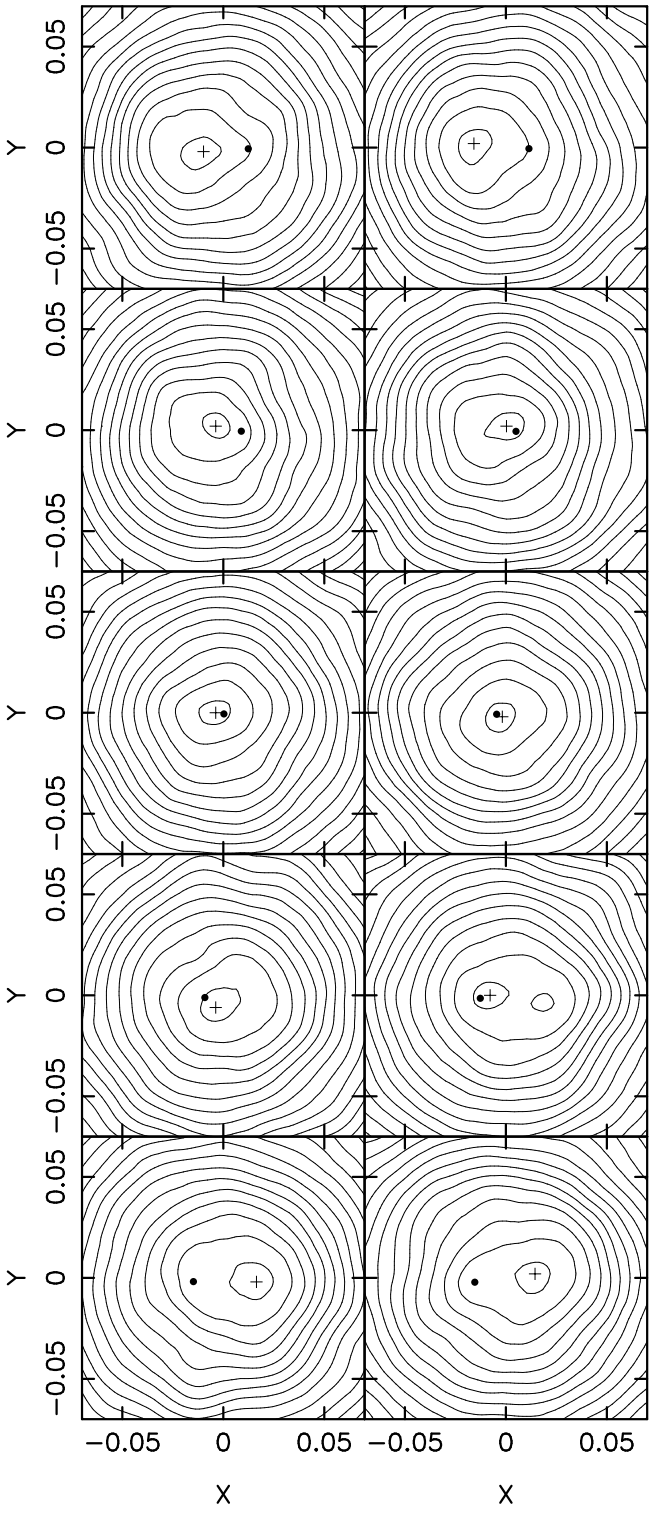

FIG. 9.— Core-BH oscillations in Phase II. This is the $N = 2 \times 10^6$ integration of Model B shown as the filled (red) circles in Fig. 8. Contours are separated by 0.034 in $\log_{10}$ of the projected density. Filled circles mark the BH and crosses mark the approximate location of the (projected) stellar density maximum. Times are $t = 2.1875, 2.21875, 2.25, ...2.46875$, increasing from upper left to lower right. The elapsed time in this figure spans approximately 1/2 oscillation period of the BH.

of the core as a whole, at roughly the same frequency as core internal frequencies, drives the oscillations.

A number of other N-body studies have noted a decrease in the effective value of $\ln\Lambda$ once a massive object has spiraled into a constant-density core. Typically the observed decrease is modest, a factor$\sim 2-3$ or so (Bontekoe & van Albada 1987; Bontekoe 1988; Weinberg 1989; Cora et al. 1997), although one recent study (Read et al. 2006) found a nearly complete disappearance of dynamical friction after the infalling particle reached the core. Read et al. proposed that the apparent vanishing of the dynamical friction force in their simulations could be explained by the degeneracy of orbital frequencies in the harmonic-oscillator potential corresponding to a precisely flat, central density profile. In such models, Read et al. found that the disappearance of the dynamical friction force was critically dependent on whether the plane defined by the inspiralling particle's orbit remained fixed; precession, induced e.g. by finite-N perturbations, caused dynamical friction to turn on again, though at a rate much slower than expected from Chandrasekhar friction. While Read et al. did consider the effect of varying the initial log-slope of the background distribution, their models were always spherical. The cores in our models are not precisely flat nor are our models precisely spherical (once the BH particle has been ejected) and these differences (coupled with the fact that the gravitational potential of the core is highly oscillatory in Phase II) may explain why we do not observe the dramatic stalling reported by Read et al. In any case, the apparent lack of an N-dependence in our simulations (Figure 8) suggests that the critical difference between our results and those of Read et al. is not particle number.

The Phase II oscillations were clearly visible in every integration with $V_{\rm kick} \geq 0.4V_{\rm esc}$. For $V_{\rm kick} = 0.3V_{\rm esc}$ there were hints of a delayed return to the Brownian regime in some of the integrations (e.g. Fig. 6) but not to the extent that we were able to estimate damping times. We could not detect the Phase II oscillations at all for $V_{\rm kick} \leq 0.2V_{\rm esc}$; in these integrations, the BH kinetic energy appears to drop very rapidly after the return to the core, more or less as expected based on the analytic model presented above or by an extrapolation of the behavior in Phase I. In any case, we assume in the remainder of this paper that the Phase II oscillations are absent when $V_{\rm kick} \leq 0.3V_{\rm esc}$. Integrations with much larger N might modify this conclusion.

The occasional *increase* in the amplitude of the Phase II oscillations, which is seen in virtually all the integrations, is suggestive of a dynamical instability (Tremaine 2005). However an instability would presumably act even in the case of small kicks, while as noted above, Phase II oscillations appear to be absent for $V_{\rm kick} \lesssim 0.3V_{\rm esc}$. We speculate that the BH must be kicked completely out of the core in order for the BH-core oscillations to be excited, as suggested by Miller & Smith (1992). The roughly sinusoidal variations in the envelope of $V^2(t)$, with a much lower frequency than ω_c, could naturally be explained in terms of beating, e.g. between the frequency of motion in the core and the frequency at which the core itself oscillates in the galactic potential.

Figures 6 and 8 suggest that the core-BH oscillations in Phase II decay roughly as an exponential in time, at least when viewed through a window of several orbital periods or longer. We investigated a number of ways to quantify the time constant τ associated with the energy damping:

1. Plots of BH energy versus time (equation 8, Fig. 3) were found not to be very useful in this regard since the total

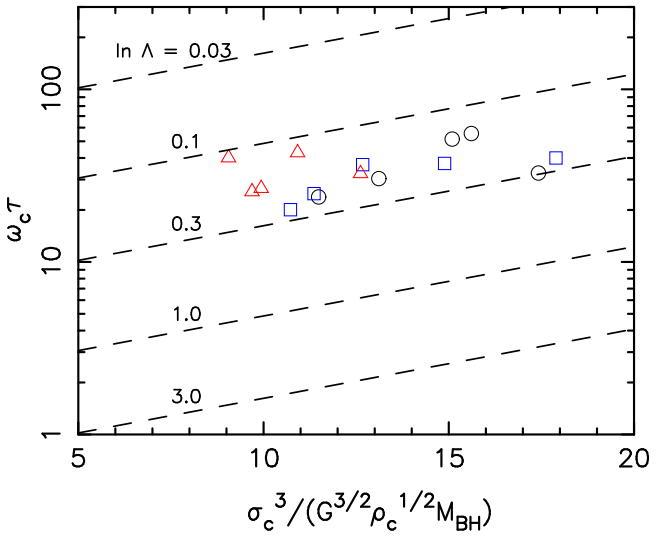

FIG. 10.— Energy-decay time constants τ for the BH in Phase II, for models A1 (black/circles), A2 (blue/squares) and B (red/triangles).

energy is dominated by the potential energy which exhibits fairly large fluctuations from time step to time step.

2. In a constant-density core, the unperturbed motion is simple harmonic oscillation with frequency ω and energy

$$E_{\rm SHO} = \frac{1}{2}\sum_{i=1}^{3}\left(\omega^2 X_i^2 + V_i^2\right).$$

We determined the dominant frequency of the BH's motion in Phase II by carrying out discrete Fourier transforms of the complex functions $X_i(t)+iV_i(t)$ and constructing power spectra (e.g. Laskar 1990). Least-squares fits to $\ln E_{\rm SHO}$ vs. t were then carried out to find the damping time constant. This approach was reasonably objective and robust, but can be criticized on the grounds that the core density is not constant and the density center is moving with time (Fig. 9), making the interpretation of $E_{\rm SHO}$ problematic.

3. Given the difficulties with evaluating and interpreting the total energy of the BH, we chose in the end to quantify the energy damping purely in terms of the the BH's kinetic energy. As noted above (Fig. 8 and associated text), $V^2(t)$ exhibits a nicely exponential decay with a well-defined time constant, and the decay is observed to continue over ~ 2 decades in kinetic energy in the case of the simulation with the largest N, until the BH's kinetic energy reaches the Brownian value. We evaluated the associated time constant by carrying out least-squares fits of $\ln V^2$ to time, yielding the coefficients (V_I^2, τ) in the expression

$$V^2(t) \approx V_I^2\, e^{-(t-T_I)/\tau}. \qquad (20)$$

Table 2 gives the τ values derived from this method. We present results only from N-body integrations with $V_{\rm kick} \geq 0.4 V_{\rm esc}$ since the smaller kicks did not excite distinct BH-core oscillations, as discussed above. To the extent that the motion approximates a damped SHO, the energy damping time is identical to the time constant for decay of the kinetic energy alone, and henceforth we will refer to τ as the "energy damping time constant." However in practice, we will use equation (20) only to predict changes in $\langle V^2\rangle$.

The energy damping times in Table 2 can immediately be scaled to physical units using equation (2). Such a scaling presumes that the core properties of our N-body models – which presumably determine τ – are related to global properties in the same way as in real galaxies. A better scheme would relate τ directly to the parameters $(\rho_c, \sigma_c, M_{\rm BH})$ that describe the conditions in the core. Since we do not understand the mechanism(s) responsible for the orbital damping in Phase II, we experimented with several ways of plotting τ versus core parameters.

TABLE 2
TIMES ASSOCIATED WITH THE EVOLUTION IN PHASES I AND II

$V_{\rm kick}/V_{\rm esc}$	T_I	τ	T_{II}	T_{II}, $N_{\rm gal}$ = ... 3×10^9	3×10^{10}	3×10^{11}	3×10^{12}
				A1			
0.1	0.3	–	–	–	–	–	–
0.2	0.3	–	–	–	–	–	–
0.3	0.3	–	–	–	–	–	–
0.4	0.4	1.6	2.9	16.8	20.5	24.2	27.9
0.5	0.7	1.3	3.2	14.5	17.5	20.5	23.4
0.6	1.5	1.9	4.6	21.1	25.5	30.0	34.2
0.7	3.0	3.4	5.8	35.3	43.2	51.0	58.8
0.8	7.3	3.8	8.5	41.6	50.3	59.0	67.8
0.9	20.2	2.5	6.5	28.3	34.0	39.8	45.5
				A2			
0.1	0.3	–	–	–	–	–	–
0.2	0.3	–	–	–	–	–	–
0.3	0.3	–	–	–	–	–	–
0.4	0.4	1.0	1.5	10.2	12.5	14.8	17.1
0.5	0.7	0.95	1.9	10.2	12.4	14.5	16.7
0.6	1.3	1.3	3.4	14.7	17.7	20.6	23.6
0.7	2.7	2.1	4.4	22.7	27.5	32.3	37.2
0.8	6.5	2.4	4.6	25.4	31.0	36.5	42.0
0.9	20.0	2.8	6.7	31.1	37.5	43.9	50.4
				B			
0.1	0.5	–	–	–	–	–	–
0.2	0.5	–	–	–	–	–	–
0.3	0.5	–	–	–	–	–	–
0.4	0.55	2.2	3.9	23.0	28.1	33.2	38.2
0.5	0.7	2.8	6.7	31.1	37.5	43.9	50.4
0.6	1.3	2.6	10.8	33.4	39.4	45.3	51.4
0.7	2.3	2.9	10.1	35.3	42.0	48.7	55.3
0.8	4.5	5.2	14.7	60.0	71.9	83.9	95.8
0.9	11.5	4.3	14.9	52.3	62.2	72.1	82.0

Figure 10 shows that a reasonably tight correlation exists when $\omega_c\tau$ is plotted against $\sigma_c^3/(G^{3/2}\rho_c^{1/2}M_{\rm BH})$. This is the expected dependence if dynamical friction is responsible for the damping (cf. equation 15). However, the effective value of $\ln\Lambda$ needed to produce the measured damping times is very small, $0.1 \lesssim \ln\Lambda \lesssim 0.3$ (Figure 10). This is yet another way of stating that orbital decay in Phase II is much slower than predicted by Chandrasekhar's formula – roughly a factor 10–20, if we adopt $\ln\Lambda \approx 2.5$ for the expected value of the Coulomb parameter (Fig. 5).

In terms of this scaling, Figure 10 allows us to express the damping times in Phase II as

$$\tau \approx 15\frac{\sigma_c^3}{G^2\rho_c M_{\rm BH}} \qquad (21)$$

$$\approx 3\times10^7{\rm yr}\left(\frac{\sigma_c}{200\,{\rm km\,s^{-1}}}\right)^{-3.86}\left(\frac{r_c}{30\,{\rm pc}}\right)^2 \qquad (22)$$

where the second line uses the $M_{\rm BH}-\sigma$ relation (Ferrarese & Ford 2005). Based on Figure 8 and on the other arguments given above, we expect the scaling in equation (22) to be independent of N, i.e. of stellar mass.

Table 2 also gives estimates of T_{II}, the elapsed time in Phase II. We defined T_{II} as the time, measured from the end of Phase I, required for the BH's velocity to fall to its rms value in Phase III, assuming the time dependence of equation (20). Table 2 shows that T_{II} is typically longer than T_I.

In a galaxy with $\gg 10^6$ stars, $V^2_{\rm Brown}$ would be much lower, and T_{II} correspondingly longer, than in our models. Assuming that the exponential dependence of energy on time persists to arbitrarily low values of E, the additional time spent in Phase II would be

$$\tau \ln\left(N_{\rm gal}/N\right) \tag{23}$$

where $N_{\rm gal}$ is the number of stars in the galaxy. We used the set of N-body simulations in Figure 8 to test this dependence. According to equation (23), doubling the number of particles should extend the elapsed time in Phase II by an additive amount of $\tau \ln 2 = 0.693\tau \approx 2.2$, given that the mean τ value for the four integrations is 3.2. Figure 8 confirms this prediction for $0.25\times 10^6 \le N \le 2\times 10^6$.

Accordingly, Table 2 also gives values of T_{II} calculated from this formula, for $N_{\rm gal} = (3\times 10^9, 3\times 10^{10}, 3\times 10^{11}, 3\times 10^{12})$. Conversion from the N-body units of Table 2 to years is discussed in § 6.

The exponential nature of the damping implies that the distribution of displacements during Phase II is approximately uniform in $\ln \Delta r$.

4. EFFECTS ON THE STELLAR DISTRIBUTION

The displacement of the BH due to gravitational radiation recoil affects the stellar distribution and therefore the density profile of the host galaxy. We expect the stellar structure inside the core to be particularly affected by the motion of the BH, with important implications for the shape of the brightness profile in the inner region. In order to evaluate the changes induced by the escaping BH, we constructed spatial and projected density profiles for all models at the end of the simulations, when the BH is well into the Brownian regime.

Figure 11 shows the space (left plots) and projected (right plots) density profiles in models A1, A2, B for $V_{\rm kick} = (0.1, 0.3, 0.5, 0.9)V_{\rm esc}$. We constructed these density profiles using the kernel-based algorithm of Merritt et al. (2006a). Particle positions were first shifted to coordinates that placed the BH at the origin. The algorithm uses an angle-averaged Gaussian kernel and modifies the kernel width based on a pilot (nearest-neighbor) estimate of the density in order to maintain a roughly constant ratio of bias to variance in the final density profile. The projected density $\Sigma(R)$ was computed via numerical projection of the space density. In order to reduce the noise still further, we combined multiple snapshots at late times and performed the fit on the combined data sets.

Figure 11 shows that a large core develops in the simulations due to the escape of the BH and its several passages through the central region. As the BH oscillates under the effect of the kick, it transfers energy to the surrounding stars, thus pushing them to larger distances. The stellar density in the core drops and the slope of the inner distribution decreases, leaving an inner profile that is flatter than the initial one. The amount of flattening in the profile or, equivalently, the mass deficit with respect to the initial profile (shown in the figure with the black solid lines), increases monotonically with the kick velocity.

It is interesting to assess whether the final N-body profiles are consistent with the core-Sérsic law, which is commonly fit to galaxies with evacuated cores (Graham et al. 2003). The core-Sérsic law is:

$$\Sigma(R) = \Sigma' \left[1+\left(\frac{r_{\rm b}}{R}\right)^{\alpha}\right]^{\gamma/\alpha} e^{-b\left[\left(R^\alpha + r_{\rm b}^\alpha\right)/R_{\rm e}^\alpha\right]^{1/n\alpha}}, \tag{24}$$

$$\Sigma' = \Sigma_b\, 2^{-\gamma/\alpha}\, e^{b\left(2^{1/\alpha} r_{\rm b}/R_{\rm e}\right)^{1/n}}, \tag{25}$$

where Σ_b is the density at the break radius r_b and the other parameters are as in equations (2) and (3). To carry out the fits in a manner as similar as possible to the procedure followed by observers, we counted the projected particle positions in bins equally spaced in $\log R$. The parameters $(R_{\rm e}, r_{\rm b}, \alpha, n, \Sigma')$ were then varied until the summed residuals in $\mu = -2.5\log\Sigma$ were minimized.

TABLE 3
FIT PARAMETERS FOR MODELS A1, A2 AND B.

$V_{\rm kick}$	$r_{\rm b}$	n	α	γ	$R_{\rm e}$	Σ_b
			A1			
0.1	0.013	4.04	3.1	0.21	0.93	6.3
0.2	0.016	4.05	4.2	0.24	0.93	5.6
0.3	0.017	4.05	4.1	0.19	0.93	5.4
0.4	0.018	4.06	3.7	0.14	0.93	5.1
0.5	0.019	4.06	3.6	0.11	0.93	4.9
0.6	0.020	4.06	3.5	0.08	0.93	4.6
0.7	0.021	4.07	3.1	0.04	0.92	4.3
0.8	0.022	4.07	2.8	0.02	0.92	4.1
0.9	0.024	4.05	2.9	0.05	0.93	3.9
			A2			
0.1	0.014	4.04	7.4	0.34	0.93	6.5
0.2	0.015	4.04	6.7	0.31	0.93	6.2
0.3	0.016	4.04	6.5	0.25	0.92	5.9
0.4	0.015	4.05	3.5	0.14	0.92	5.9
0.5	0.017	4.05	4.0	0.12	0.92	5.4
0.6	0.019	4.05	4.2	0.16	0.92	4.9
0.7	0.018	4.07	2.7	0.08	0.92	4.9
0.8	0.022	4.06	3.6	0.07	0.92	4.4
0.9	0.026	4.07	4.1	0.11	0.92	3.9
			B			
0.1	0.020	4.05	1.9	0.16	0.92	4.4
0.2	0.026	4.04	2.9	0.20	0.93	3.8
0.3	0.030	4.04	3.7	0.20	0.93	3.4
0.4	0.034	4.05	4.3	0.16	0.92	3.1
0.5	0.034	4.06	3.1	0.12	0.92	3.0
0.6	0.035	4.06	3.0	0.09	0.92	2.8
0.7	0.039	4.08	3.0	0.07	0.91	2.6
0.8	0.042	4.08	2.9	0.05	0.91	2.4
0.9	0.044	4.09	2.6	0.02	0.91	2.3

The best-fit parameters for models A1, A2 and B are listed in Table 3. Three of the best fits for model A1 are shown in Figure 12 (lines) together with the projected density profiles computed from the N-body data (points).

It appears that the host galaxies to recoiling BHs are well represented by core-Sérsic profiles. In particular, the fits show, once again, that the core tends to expand as the BH oscillates in and out of it, and that the final core size scales as $r_b \sim M_{\rm BH} V_{\rm kick}^{\beta}$, with $0.3 \lesssim \beta \lesssim 0.6$. In addition, the transition from the inner power law to the outer Sérsic profile is rather sharp, with best-fit values of α in the range $2 \lesssim \alpha \lesssim 7$. The initial $n = 4$ de Vaucouleurs outer slope is not substantially modified by the BH.

A flattening of the inner profile is also observed in the simulations of Boylan-Kolchin et al. (2004), who follow the evolution of a spherical stellar bulge with a recoiling central black hole using an N-body tree code. They find that the density profile of the system evolves as a consequence of the gravi-

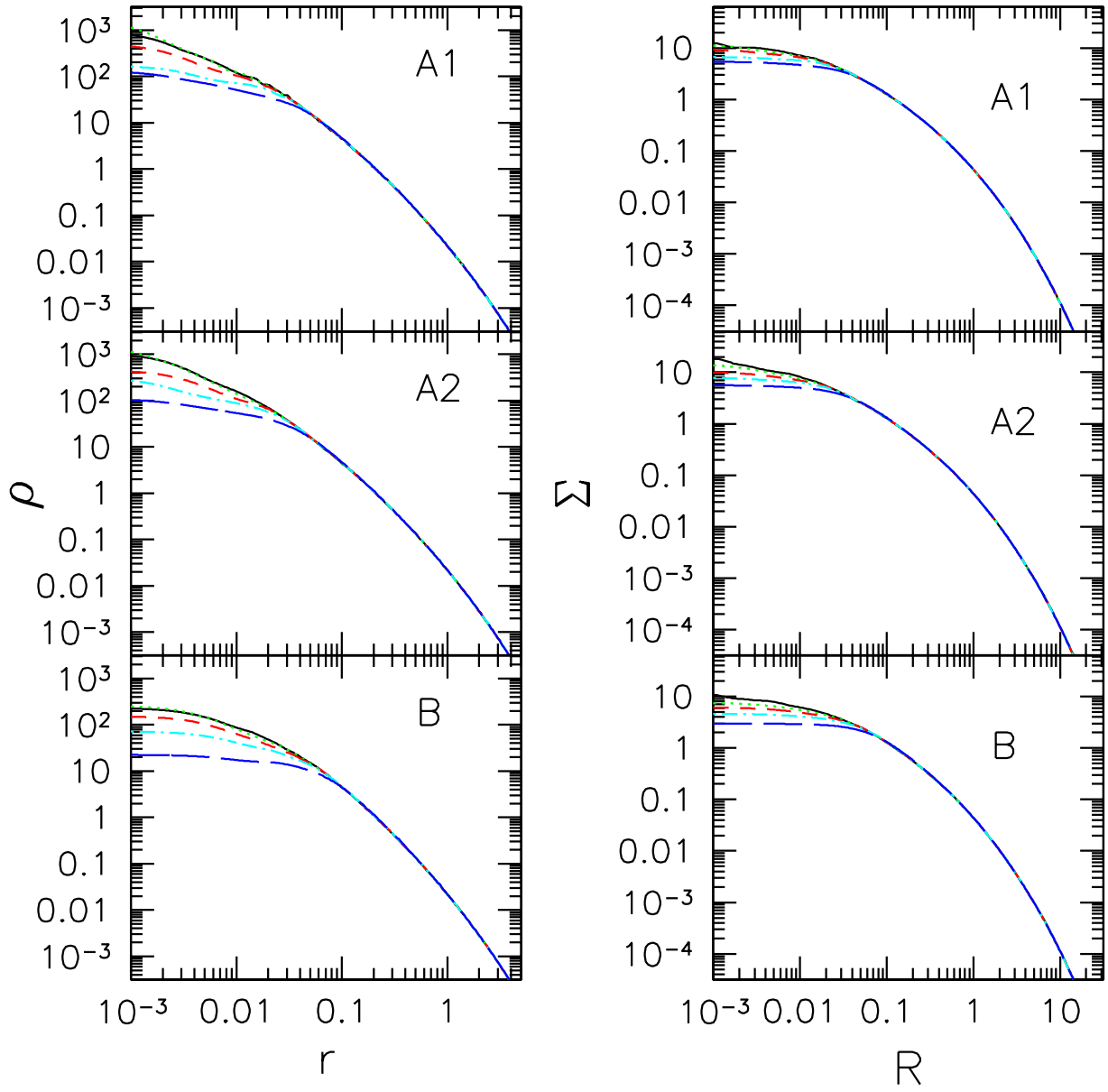

FIG. 11.— Space (left) and projected (right) density profiles for models A1, A2 and B and different values of the kick velocity: $V_{\rm kick} = 0.1\,V_{\rm esc}$ (green/dotted), $V_{\rm kick} = 0.3\,V_{\rm esc}$ (red/dashed), $V_{\rm kick} = 0.5\,V_{\rm esc}$ (cyan/dot-dashed), $V_{\rm kick} = 0.9\,V_{\rm esc}$ (blue/long dashed). The black solid lines represent the initial profile, which is the same for each value of $V_{\rm kick}$.

tational radiation recoil and flattens substantially. A core of size equal to the BH sphere of influence forms on a relatively short time-scale, and remains even after several dynamical times. A flattening of the profile is observed for recoil velocities smaller and larger than the central escape speed, though an additional flattening is present if the black hole returns to the core after the ejection.

A measurable signature of a recoiling BH is the mass deficit, the net mass removed from the central regions (Milosavljević et al. 2002). Mass deficits produced by recoil will add to the depletion caused by the pre-existing BH binary, which ejects stars from the core during close encounters. The deficit produced by the binary is proportional to the mass of the binary, with only a weak dependence on the mass ratio and the initial density distribution (Merritt 2006). Therefore, a binary BH can only produce a deficit $M_{\rm def} \approx M_{\rm BH}$. This could explain the peak in the distribution of observed mass deficits at $M_{\rm def}/M_{\rm BH} \approx 1$ (Graham 2004; Ferrarese et al. 2006). The tail of the distribution, however, extends to values of $M_{\rm def}/M_{\rm BH} \sim 5$. While such large values might be explained as successive mergers (Merritt 2006), a recoiling BH represents an interesting alternative.

We evaluated the mass deficits in the final N-body models by computing the difference in stellar mass, enclosed within a sphere of radius r_s, between the initial and final space density profiles. Given the fact that the deficits depend rather sensitively on the value of r_s, we computed $M_{\rm def}$ as a function of r_s for a number of models and kicks. In all cases, $M_{\rm def}$ first increases rapidly with r_s and then flattens out to an approximately constant value. Based on such tests, we concluded that

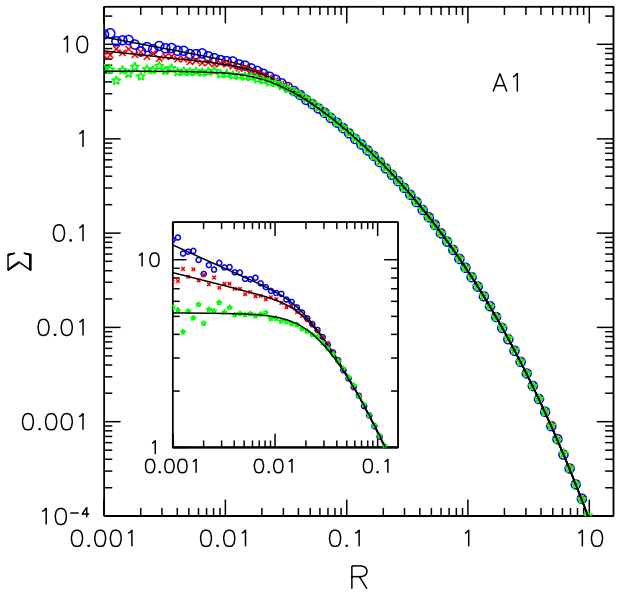

FIG. 12.— Projected density profiles for model A1 computed from the N-body data (points), compared with best-fitting core-Sérsic models (lines), for three different values of the kick velocity ($V_{\rm kick} = 0.2, 0.4, 0.8\,V_{\rm esc}$). The insert shows a zoom into the central region.

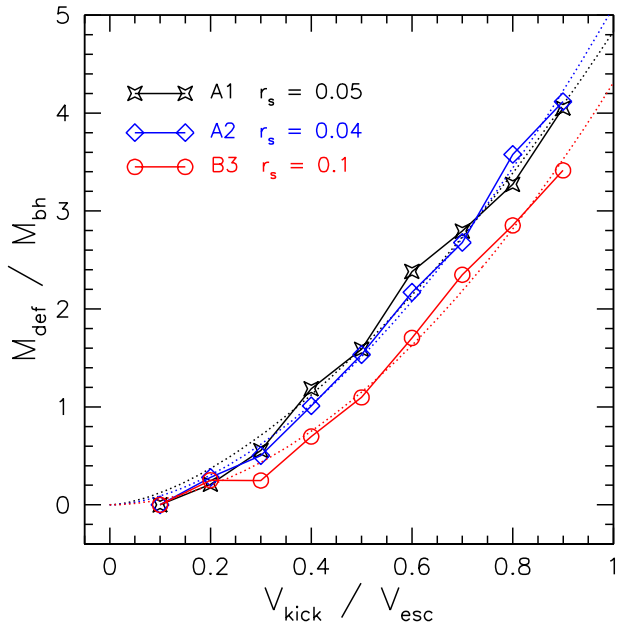

FIG. 13.— Mass deficits, as defined in the text, for the different runs: A1 (black), A2 (blue), B (red). Dashed lines show power-law fits.

the most appropriate values to use for the computation of the mass deficits were as follows: $r_s = 0.05$ for model A1, 0.04 for model A2 and 0.1 for model B. The results for all three models are shown in Figure 13. Also shown are least-squares fits to $Y = aX^b$, where $Y \equiv M_{\rm def}/M_{\rm BH}$ and $X \equiv V_{\rm kick}/V_{\rm esc}$. The best-fit parameters are:

$$\begin{aligned} \text{Model A1}: a = 4.83,\ b = 1.59 \\ \text{Model A2}: a = 5.08,\ b = 1.75 \\ \text{Model B}\ : a = 4.31,\ b = 1.90 \end{aligned} \qquad (26)$$

The largest kicks result in mass deficits as large as $4-5M_{\rm BH}$, which is consistent with the largest observed deficits (Merritt 2006). Our definition of mass deficits as the difference in integrated mass between initial and final profiles implies that our estimates do not take into account any depletion prior to the kick. One should therefore add the contribution from the binary evolution phase ($M_{\rm def} \approx 1M_{\rm BH}$) to our measured deficits before comparing with the observed values.

The sensitivity of $M_{\rm def}$ to r_s, which presumably is a feature of real luminosity profiles as well, suggests that a more objective way be found to measure mass deficits.

We compare the projected density profiles obtained from the N-body simulations to the brightness profiles of a sample of early-type galaxies in the Virgo cluster observed with the *Advanced Camera for Surveys* (ACS) on the Hubble Space Telescope (Ferrarese et al. 2006). In this study, the authors find that, while simple Sérsic models generally provide a good representation of the global galaxy profiles, the brightest galaxies require a power-law component within a characteristic break radius and are therefore best modeled with core-Sérsic profiles.

We select two representative galaxies in the sample and compare their surface density profiles with each of the 27 final profiles obtained from the simulations (9 values of the kick velocities $0.1\ldots0.9$ for each of the 3 models A1, A2, B).

The brightest Virgo galaxy, VCC1226 (M49, NGC 4472), has the largest value of mass deficit ($M_{\rm def}/M_{\rm BH} \sim 4$) and has a Sérsic index that is not too far from our N-body models, $n \sim 5.9$[4]. On the other hand, VCC 731 (NGC 4365) has a relatively small core and a typical mass deficit of $\sim 1M_{\rm BH}$ (Merritt 2006). For each galaxy, we scale the N-body profiles to have the same r_b and $\Sigma(r_b)$ as the galaxy itself.

Figure 14 shows that the brightness profiles of both galaxies can be reasonably well fit by (at least) one of the N-body models. In particular, the profile of VCC 1226 is well fit by models with $V_{\rm kick} \geq 0.4V_{\rm esc} \approx 550\,{\rm km\,s^{-1}}$ while VCC 731 is well fit by models with $V_{\rm kick} \gtrsim 0.1V_{\rm esc} \approx 110\,{\rm km\,s^{-1}}$. This indicates that observed brightness profiles, and even the largest cores, can be well reproduced by the gravitational recoil kicks.

5. EVOLUTION TIMES IN REAL GALAXIES

Given a galaxy's effective radius $R_{\rm e}$ and total mass $M_{\rm gal}$, equations (2) relate our N-body units to physical units. We adopt the scaling relations derived from the ACS Virgo cluster survey of Côté et al. (2004) between $R_{\rm e}$ and absolute blue magnitude M_B for early-type galaxies. Ferrarese et al. (2006) found, for Virgo E galaxies fainter than $M_B \approx -20.5$, a mean relation

$$\log_{10} R_{\rm e} = 0.144 - 0.05\,(M_B + 20) \qquad (27)$$

where $R_{\rm e}$ is in kpc. (Brighter galaxies obey a different relation and are considered separately below.) We relate M_B to galaxy mass using Gerhard et al.'s (2001) expression for the mass to light ratio in the blue band:

$$\log_{10}\left[\left(\frac{M}{L}\right)\Big/\left(\frac{M}{L}\right)_{\odot}\right]_B \approx 1.17 + 0.67\log_{10}\left(\frac{L_B}{10^{11}L_{\odot,B}}\right). \qquad (28)$$

Equation (28) was derived from dynamical modeling of galaxies with $M_B \gtrsim -22.5$ and represents an average for the matter within the effective radius, including dark matter if present.

[4] Most of the bright galaxies in the ACS sample have $n \gtrsim 7$.

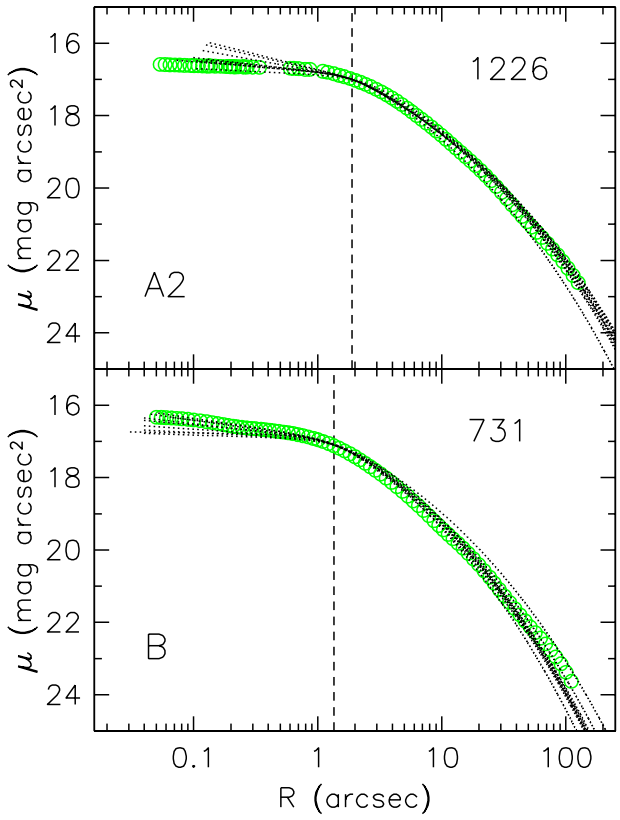

FIG. 14.— Surface brightness profiles for the Virgo galaxies VCC 1226 (top) and VCC 731 (bottom) from the ACS sample compared to the N-body profiles obtained from the best fitting of the three models. The different lines correspond to the 9 different kicks $V_{\rm kick}/V_{\rm esc} = 0.1 \ldots 0.9$.

Combining these relations gives

$$R_{\rm e} \approx 1.2\ {\rm kpc} \left(\frac{M_{\rm gal}}{10^{10}\,{\rm M}_\odot}\right)^{0.075}. \qquad (29)$$

The dependence of $R_{\rm e}$ on $M_{\rm gal}$ is weak, a consequence of the low slope of the $R_{\rm e} - M_B$ relation. However we note that the scatter in this relation is large (e.g. Ferrarese et al. 2006, Fig. 136).

Some fiducial values, and their implied N-body scalings (from equation 2), are:

$$\begin{aligned}
M_{\rm gal} &= 3\times10^9\,{\rm M}_\odot \quad R_{\rm e} = 1.1\ {\rm kpc} \\
&\quad [T] = 1.0\times10^7{\rm yr} \quad [V] = 110\,{\rm km\,s^{-1}}, \\
M_{\rm gal} &= 3\times10^{10}\,{\rm M}_\odot \quad R_{\rm e} = 1.3\ {\rm kpc} \\
&\quad [T] = 4.1\times10^6{\rm yr} \quad [V] = 315\,{\rm km\,s^{-1}}, \\
M_{\rm gal} &= 3\times10^{11}\,{\rm M}_\odot \quad R_{\rm e} = 1.5\ {\rm kpc} \\
&\quad [T] = 1.7\times10^6{\rm yr} \quad [V] = 910\,{\rm km\,s^{-1}}.
\end{aligned}$$

The trend of decreasing $[T]$ with increasing $M_{\rm gal}$ reflects the well-known higher density of more massive galaxies (Graham et al. 2003). The central escape velocities in our models are $2.0 \lesssim V_{\rm esc} \lesssim 2.2$ in N-body units, corresponding to $V_{\rm esc} \approx 2.1\times[V] \approx 2000\,{\rm km\,s^{-1}}$ when scaled to a $3\times10^{11}\,{\rm M}_\odot$ galaxy. This agrees well with escape velocities of bright E-galaxies derived from more detailed modeling (e.g. Fig. 2, Merritt et al. 2004).

All of the times listed in Table 2 can be scaled to physical units using these relations. Figure 15 shows the result for the three fiducial values of $M_{\rm gal}$. We have used equation (23) to correct the measured T_{II} values to different values of $N_{\rm gal} \equiv M_{\rm gal}/m_\star$ assuming $m_\star = {\rm M}_\odot$; we also show, as conservative lower limits, the T_{II} times obtained directly from the simulations.

Figure 15 seem to suggest that return times depend discontinuously on $V_{\rm kick}$, since Phase II does not appear to exist in our simulations when $V_{\rm kick} \lesssim 0.3 V_{\rm esc}$. As discussed above, this might not be true in simulations with larger N, or in real galaxies. In any case, for $V_{\rm kick} \gtrsim 0.4 V_{\rm esc}$, return times are dominated by the time spent in Phase II ("BH-core oscillations").

The brightest galaxies, $M_B \lesssim -21$, appear to obey a different scaling relation between $R_{\rm e}$ and M_B than the relation (29) given above (Ferrarese et al. 2006). Furthermore, these bright galaxies are typically fit by Sérsic indices in the range $5 \lesssim n \lesssim 10$, larger than the value $n = 4$ adopted here for the N-body models. On the other hand, the brightest E galaxies often have resolved cores with well-determined sizes and densities (cf. § 4). Furthermore, equation (22) gives the damping time τ in Phase II in terms of core properties alone.

We define the Phase II return times for these galaxies as the time for the BH's energy to decrease from

$$\frac{1}{2}\omega_c^2 r_c^2 \approx \frac{2}{3}\pi G \rho_c r_c^2, \qquad (30)$$

the BH's energy when it first re-enters the core, to

$$\frac{1}{2}V_{\rm brown}^2 \approx \frac{3}{2}\frac{m_\star}{M_{\rm BH}}\sigma_c^2, \qquad (31)$$

the Brownian energy, assuming an energy damping time constant of τ; for the latter we take equation (22). This time is

$$\begin{aligned}
T_{II} &= \mathcal{N}\tau, \\
\tau &\approx 15\frac{\sigma_c^3}{G^2\rho_c M_{\rm BH}} \qquad (32) \\
&\approx 1.2\times10^7{\rm yr}\left(\frac{\sigma_c}{250\,{\rm km\,s^{-1}}}\right)^3\left(\frac{\rho_c}{10^3\,{\rm M}_\odot\,{\rm pc^{-3}}}\right)^{-1}\left(\frac{M_{\rm BH}}{10^9\,{\rm M}_\odot}\right)^{-1}, \\
\mathcal{N} &= \ln\left(\frac{1}{F^2}\frac{M_{\rm BH}}{m_\star}\right) \\
&\approx \ln\left(\frac{1}{F^2}\frac{M_{\rm BH}}{M_{\rm gal}}\frac{M_{\rm gal}}{{\rm M}_\odot}\right), \qquad (33)
\end{aligned}$$

with $F \approx 2$ the form factor defined above, and we have again assumed $m_\star = {\rm M}_\odot$.

Figure 16 shows estimates of τ and $\mathcal{N}\tau$ for the six brightest galaxies in the ACS Virgo sample excluding M87, which has an active nucleus (Côté et al. 2004). Of course, this figure is only meaningful under the assumption that the BHs in these galaxies have received large enough kicks to remove them completely from the core, i.e. $V_{\rm kick} \approx 10^3\,{\rm km\,s^{-1}}$. But if this did occur, Figure 16 suggests that return times would be of order 1 Gyr. Such a long time is comparable with the mean time between galaxy mergers in a dense environment like the Virgo cluster. Hence, a SMBH might never return fully to the center before another SMBH spirals in.

6. OBSERVABLE CONSEQUENCES

6.1. *Likelihood of Large Kicks*

Kicks large enough to remove SMBHs from cores, $V_{\rm kick} \gtrsim 0.4 V_{\rm esc}$, range from $\sim 90\,{\rm km\,s^{-1}}$ for $M_{\rm gal} = 3\times10^9\,{\rm M}_\odot$, to $\sim 750\,{\rm km\,s^{-1}}$ for $M_{\rm gal} = 3\times10^{11}\,{\rm M}_\odot$, to $\sim 1000\,{\rm km\,s^{-1}}$ for $M_{\rm gal} = 3\times10^{12}\,{\rm M}_\odot$, based on the fiducial scalings in § 5. The

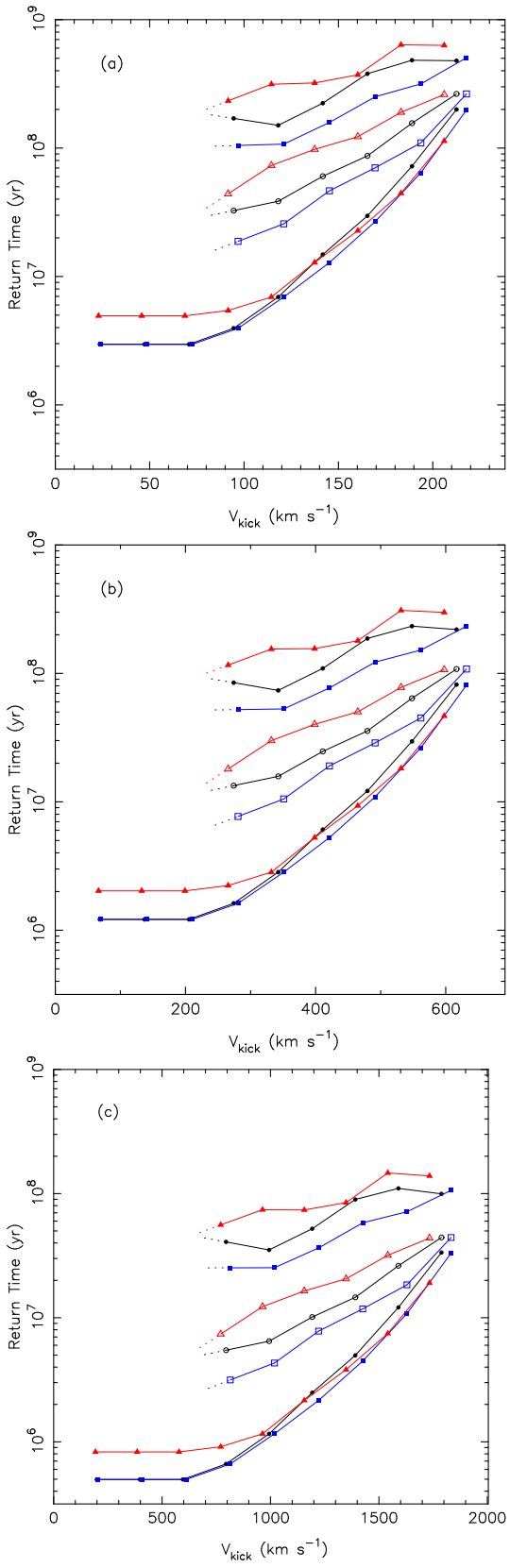

FIG. 15.— Return times of kicked BHs. These are plots of the N-body values given in Table 2, scaled to physical units using equations (2) and (29). *Lower (filled) symbols:* T_I; *Middle (open) symbols:* $T_I + T_{II}$, with T_{II} taken directly from the simulations; *Upper (filled) symbols:* $T_I + T_{II}$, with T_{II} scaled to $N_{\rm gal}$ using equation (23). (a) $M_{\rm gal} = 3\times10^9\,{\rm M}_\odot$; (b) $M_{\rm gal} = 3\times10^{10}\,{\rm M}_\odot$; (c) $M_{\rm gal} = 3\times10^{11}\,{\rm M}_\odot$.

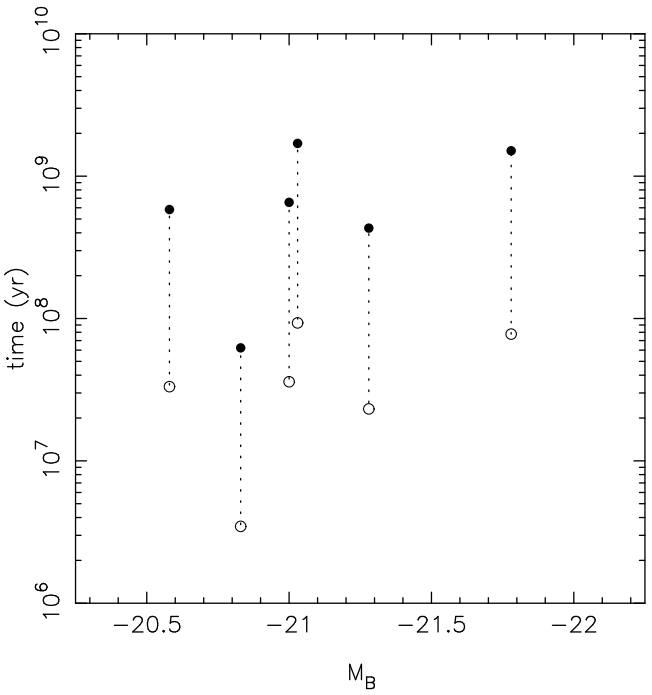

FIG. 16.— Estimates of the return time in Phase II for supermassive black holes in the six brightest Virgo galaxies, excluding M87 (Côté et al. 2004). This plot assumes that the SMBHs have received a kick large enough to remove them from the core initially. Lower (open) symbols show the energy decay time constant in the core, τ (equation 32), while upper (filled) symbols show $\mathcal{N}\tau$, where $\mathcal{N}$ is the estimated number of time constants required for the BH's velocity to decay to the Brownian value (equation 33).

most propitious configuration for the kicks appears to be an equal-mass binary in which the individual spin vectors are oppositely aligned and oriented parallel to the orbital plane (Campanelli et al. 2007a; González et al. 2007a). Assuming this most favorable orientation, and setting the spins to their maximal values, the maximum kick (oriented parallel to the binary angular momentum vector) is believed to scale with binary mass ratio $q \equiv M_2/M_1 \leq 1$ as

$$V_{\rm max} \approx 6\times10^4 {\rm km\ s^{-1}} \frac{q^2}{(1+q)^4} \qquad (34)$$

(Campanelli et al. 2007c). Mass ratios as small as $q \approx 0.2$ can therefore result in kicks $\gtrsim 1000$ km s^{-1}. While the assumption of near-maximal spins is probably not an extreme one (e.g. Shapiro 2005; Gammie et al. 2004), orienting the BHs with their spins perpendicular to the orbital angular momentum may seem odd, particularly in gas-rich galaxies (Bogdanović et al. 2007). However there is considerable circumstantial evidence that SMBH spin axes bear no relation to the orientations of the gas disks that surround them (Kinney et al. 2000; Gallimore et al. 2006; Borguet et al. 2007) and this is presumably even more true with respect to the directions of infalling BHs in gas-free galaxies. If SMBH spins do orient parallel with orbital angular momenta, the maximum kick is more modest and contains contributions from both the "mass asymmetry" ($M_1 \neq M_2$) and from the spins. The two kick components, both of which are parallel to the orbital plane, are believed to be approximately

independent and to scale roughly as

$$V_{\rm mass} \approx V_1 \frac{q^2(1-q)}{(1+q)^5}, \quad (35)$$

$$V_{\rm spin} \approx V_2 \frac{q^2}{(1+q)^5}(\alpha_2 - q\alpha_1); \quad (36)$$

$V_1 \approx V_2 \approx 10^4$ km s^{-1} and α denotes a dimensionless spin, $-1 \le \alpha \le 1$ (Campanelli et al. 2007c; Baker et al. 2007; Lousto & Zlochower 2007). $V_{\rm mass}$ peaks at ~ 200 km s^{-1} for $q \approx 0.4$ while $V_{\rm spin}$ peaks at ~ 600 km s^{-1} for $q \approx 1, \alpha_1 = -\alpha_2 = 1$. In this less-favorable configuration, kicks could remove SMBHs only from the cores of low-to-moderate luminosity galaxies. Estimates of the kick velocity distribution (e.g. Schnittman & Buonanno 2007) are extremely uncertain since they depend on the unknown distributions of SMBH mass ratios, spins and spin orientations. In what follows, we will focus on the consequences of kicks that are large enough to remove SMBHs from galaxy cores and to excite the long-lived oscillations that we described above.

6.2. *Offset and Double Nuclei*

Lauer et al. (2005) identified five galaxies in which the point of maximum surface brightness is displaced from the center of the isophotes defined by the galaxy on large scales. All are luminous, "core" galaxies. Contour plots for two of the galaxies, NGC 507 and 1374 (Figs. 17, 18 of Lauer et al. 2005), look strikingly similar to the "Phase II" isodensity plots in Figure 9. Displacements are cited for NGC 507 ($0''.06 \approx 19$pc), NGC 1374 ($0''.02 \approx 2.1$pc), and NGC 7619 ($0''.04 \approx 11$pc), all of which are of order the core radii in these galaxies. The five galaxies with offset nuclei comprise 12% of the Lauer et al. "core" galaxy sample; no offset nuclei were found among the "power-law" (non-cored) galaxies. Several of the offsets are close to the resolution limit, and some offsets might go unobserved due to projection, so it is likely that offset nuclei are quite common in "core" galaxies. If the offsets are produced by oscillations like those in Figure 9, the SMBHs in these galaxies would be located on the opposite side of the galaxy photocenter from the point of peak brightness. Phase II oscillations can also produce a "double nucleus" morphology (e.g. Figure 9, frame 8) with the BH located at either the higher or secondary peak. This is a reasonable model for the double nucleus in NGC 4486B (Lauer et al. 1996), since the two peaks are closely matched in brightness and are offset by similar amounts (~ 6pc) from the galaxy photocenter. Galaxies with central minima in the surface brightness (e.g. NGC 4406, NGC 6876; Lauer et al. (2002)) might also be explained in this way. This model is probably not as appropriate for the more famous double nucleus in M31, since M31 is not a "core" galaxy, and one of the brightness peaks (the one associated with the SMBH) lies close to the galaxy photocenter (Lauer et al. 1993).

6.3. *Displaced AGN*

An ejected SMBH can appear as a spatially or kinematically displaced AGN (Kapoor 1976, 1983a,b). A recoiling SMBH retains gas that is orbiting around it within a distance

$$r_{\rm eff} \approx \frac{GM_{\rm BH}}{V_{\rm kick}^2} \approx 0.5\,{\rm pc}\, M_8 V_{\rm k,1000}^{-2} \quad (37)$$

with $M_8 \equiv M_{\rm BH}/10^8\,{\rm M}_\odot$ and $V_{\rm k,1000} \equiv V_{\rm kick}/1000\,{\rm km\,s^{-1}}$. An accretion disk if present would mostly be retained, and for kicks $\lesssim 10^3\,{\rm km\,s^{-1}}$, $r_{\rm eff}$ is large enough to encompass most of the broad emission-line region gas as well. Narrow emission lines originate in gas moving in the gravitational potential of the host galaxy and would not follow a recoiling SMBH (Merritt et al. 2006b). Bonning et al. (2007) used this argument to search for kinematic offsets between spectral features associated with the broad- and narrow emission line regions. No convincing cases were found. This may be a consequence of the rapid decrease in SMBH energy during Phase I (Fig. 3). In the longer-lived oscillations that characterize Phase II, the rms velocity of the SMBH drops from

$$\sim 90\,{\rm km\,s^{-1}} \left(\frac{\rho_c}{10^3\,{\rm M}_\odot\,{\rm pc^{-3}}}\right)^{1/2} \left(\frac{r_c}{30\,{\rm pc}}\right) \quad (38)$$

when it first re-enters the core, to

$$\sim 0.03\,{\rm km\,s^{-1}} \left(\frac{M_{\rm BH}}{10^8\,{\rm M}_\odot}\right)^{-1/2} \left(\frac{\sigma_c}{200\,{\rm km\,s^{-1}}}\right) \quad (39)$$

in the Brownian regime. Such small velocity offsets would be difficult to detect. An alternative approach would be to search for linear displacements ΔR between the AGN emission and the peak of the stellar surface brightness. This displacement is $\sim r_c$ at the start of Phase II, dropping to $\sim \sqrt{m_\star/M_{\rm BH}}\,r_c$ in the Brownian regime; the exponential nature of the damping implies an approximately uniform distribution of $\ln \Delta R$ during Phase II. Relatively large ($\sim 10-100$pc) offsets between the AGN and either the stellar density peak or the center of rotation have in fact been claimed in a number of galaxies based on integral-field spectroscopy (e.g. Mediavilla & Arribas 1993; Mediavilla et al. 2005).

6.4. *Wiggling Jets*

During Phase II, the SMBH oscillates sinusoidally within the core with roughly constant period,

$$\frac{2\pi}{\omega_c} \approx 1.4\times 10^6\,{\rm yr} \left(\frac{\rho_c}{10^3\,{\rm M}_\odot\,{\rm pc^{-3}}}\right)^{-1/2}, \quad (40)$$

and with velocities as given above. Such motion will induce periodic deviations in the velocity and direction of a jet emitted by the SMBH (Kaastra & Roos 1992). If the jet is oriented perpendicularly to the direction of motion of the SMBH, the jet direction is fixed, and the jet material moves on a cylindrical surface with radius equal to the radius of the SMBH's orbit. If the jet velocity has some component parallel to the SMBH's motion, the two velocities add and the cylinder becomes a cone over which the jet precesses (Roos et al. 1993). Such models have been used to explain the helical distortions observed in a number radio sources; the inferred orbital periods are typically $1-100$ yr, and the jet accelerations are usually ascribed to the orbit of the jet-producing SMBH around a second SMBH in a close ($\ll 1$pc) binary pair. However some sources are fit by models with longer periods. For instance, the morphology of the **C**-type source 3C 449 has been reproduced assuming jet forcing with a period of $\sim 10^7$ yr (Hardee et al. 1994). Such long periods are sometimes explained in terms of bulk motion of the galaxy hosting the radio source (Blandford & Icke 1978), but oscillations of the SMBH within the core might provide a tenable alternative in some cases.

6.5. *Oversized Cores and Hypermassive Black Holes*

Cores generated by kicked SMBHs can be substantially larger than those produced by "core scouring" from a binary SMBH (Milosavljević & Merritt 2001; Merritt 2006), particularly when $V_{\rm kick} \gtrsim 0.4 V_{\rm esc}$. As shown in § 4 (Figures 11-14), kick-induced cores can be as large as those observed in some of the brightest "core" galaxies, having mass deficits of $4-5M_{\rm BH}$ and core radii several times the SMBH influence radius, or $\sim 5\%$ of the galaxy's half-light radius. (Similar conclusions were reached already by Boylan-Kolchin et al. (2004) and Merritt et al. (2004).) While the majority of observed mass deficits lie in the range $0.5 \lesssim M_{\rm def}/M_{\rm BH} \lesssim 1.5$, some E galaxies have $M_{\rm def}/M_{\rm BH} \gtrsim 3$, too large to be easily explained by core scouring. Lauer et al. (2007) invoked the oversized cores, along with other circumstantial evidence, to argue that the SMBHs in the brightest E galaxies are "hypermassive," $M_{\rm BH} \gtrsim 10^{10}\,{\rm M}_\odot$. An alternative possibility is that the largest cores have been enlarged by kicks. Figure 13, combined with earlier N-body results (Merritt 2006), suggests that the total mass deficit generated by a binary SMBH following a single galaxy merger is

$$\begin{aligned} M_{\rm def} &= M_{\rm def,bin} + M_{\rm def,kick} \\ M_{\rm def,bin} &\approx 0.7 q^{0.2} M_{\rm BH}, \\ M_{\rm def,kick} &\approx 5 M_{\rm BH} \left(V_{\rm kick}/V_{\rm esc}\right)^{1.75} \end{aligned} \tag{41}$$

where $M_{\rm def,bin}$ and $M_{\rm def,kick}$ are the mass deficits generated by "core scouring" and by the kick respectively and $q \equiv M_2/M_1 \leq 1$ is the binary mass ratio. It has been argued (Merritt 2006) that the ratio $M_{\rm def,bin}/M_{\rm BH}$ increases in multiple mergers, and the same is likely to be true for kick-induced core growth. Thus, the decrease in typical values of of $V_{\rm kick}/V_{\rm esc}$ with increasing galaxy luminosity might be offset by the greater number of mergers that contribute to the growth of luminous galaxies, leading to comparable values of $M_{\rm def}/M_{\rm BH}$. In any case, the possibility that core growth is dominated by the kicks should be considered in future studies.

We thank D. Axon, M. Campanelli, S. Komossa, C. Lousto, R. Miller, A. Robinson and Y. Zlochower for illuminating discussions. This work was supported by grants AST-0206031, AST-0420920 and AST-0437519 from the NSF, grant NNG04GJ48G from NASA, and grant HST-AR-09519.01-A from STScI.

REFERENCES

Bahcall, J. N., & Wolf, R. A. 1976, ApJ, 209, 214
Baker, J. G., Boggs, W. D., Centrella, J., Kelly, B. J., McWilliams, S. T., Miller, M. C., & van Meter, J. R. 2007, ApJ, 668, 1140
Baker, J. G., Centrella, J., Choi, D.-I., Koppitz, M., & van Meter, J. 2006a, Physical Review Letters, 96, 111102
Baker, J. G., Centrella, J., Choi, D.-I., Koppitz, M., van Meter, J. R., & Miller, M. C. 2006b, ApJ, 653, L93
Bekenstein, J. D. 1973, ApJ, 183, 657
Bertin, G., Liseikina, T., & Pegoraro. 2003, A&A, 405, 73
Blandford, R. D., & Icke, V. 1978, MNRAS, 185, 527
Bogdanović, T., Reynolds, C. S., & Miller, M. C. 2007, ApJ, 661, L147
Bonning, E. W., Shields, G. A., & Salviander, S. 2007, ArXiv e-prints, 705
Bontekoe, T. R. 1988, PhD thesis, , Groningen Univ., (1988)
Bontekoe, T. R., & van Albada, T. S. 1987, MNRAS, 224, 349
Borguet, B., Hutsemékers, D., Letawe, G., Letawe, Y., & Magain, P. 2007, ArXiv e-prints, 710
Boylan-Kolchin, M., Ma, C.-P., & Quataert, E. 2004, ApJ, 613, L37
Campanelli, M., Lousto, C., Zlochower, Y., & Merritt, D. 2007a, ApJ, 659, L5
Campanelli, M., Lousto, C. O., Marronetti, P., & Zlochower, Y. 2006, Physical Review Letters, 96, 111101
Campanelli, M., Lousto, C. O., Zlochower, Y., Krishnan, B., & Merritt, D. 2007b, Phys. Rev. D, 75, 064030
Campanelli, M., Lousto, C. O., Zlochower, Y., & Merritt, D. 2007c, Physical Review Letters, 98, 231102
Chandrasekhar, S. 1943, ApJ, 97, 255
Cora, S. A., Muzzio, J. C., & Vergne, M. M. 1997, MNRAS, 289, 253
Côté, P., Blakeslee, J. P., Ferrarese, L., Jordán, A., Mei, S., Merritt, D., Milosavljević, M., Peng, E. W., Tonry, J. L., & West, M. J. 2004, ApJS, 153, 223
de Vaucouleurs, G. 1948, Annales d'Astrophysique, 11, 247
—. 1959, Handbuch der Physik, 53, 275
Faber, S. M., Tremaine, S., Ajhar, E. A., Byun, Y.-I., Dressler, A., Gebhardt, K., Grillmair, C., Kormendy, J., Lauer, T. R., & Richstone, D. 1997, AJ, 114, 1771
Favata, M., Hughes, S. A., & Holz, D. E. 2004, ApJ, 607, L5
Ferrarese, L., Côté, P., Jordán, A., Peng, E. W., Blakeslee, J. P., Piatek, S., Mei, S., Merritt, D., Milosavljević, M., Tonry, J. L., & West, M. J. 2006, ApJS, 164, 334
Ferrarese, L., & Ford, H. 2005, Space Science Reviews, 116, 523
Fitchett, M. J., & Detweiler, S. 1984, MNRAS, 211, 933
Fukushige, T., Makino, J., & Kawai, A. 2005, PASJ, 57, 1009
Gallimore, J. F., Axon, D. J., O'Dea, C. P., Baum, S. A., & Pedlar, A. 2006, AJ, 132, 546
Gammie, C. F., Shapiro, S. L., & McKinney, J. C. 2004, ApJ, 602, 312
González, J. A., Hannam, M., Sperhake, U., Brügmann, B., & Husa, S. 2007a, Physical Review Letters, 98, 231101
González, J. A., Sperhake, U., Brügmann, B., Hannam, M., & Husa, S. 2007b, Physical Review Letters, 98, 091101
Graham, A. W. 2004, ApJ, 613, L33
Graham, A. W., Erwin, P., Trujillo, I., & Asensio Ramos, A. 2003, AJ, 125, 2951
Hardee, P. E., Cooper, M. A., & Clarke, D. A. 1994, ApJ, 424, 126
Harfst, S., Gualandris, A., Merritt, D., Spurzem, R., Portegies Zwart, S., & Berczik, P. 2007, New Astronomy, 12, 357
Herrmann, F., Hinder, I., Shoemaker, D., & Laguna, P. 2007, Classical and Quantum Gravity, 24, 33
Just, A., & Peñarrubia, J. 2005, A&A, 431, 861
Kaastra, J. S., & Roos, N. 1992, A&A, 254, 96
Kapoor, R. C. 1976, Pramana, 7, 334
—. 1983a, Ap&SS, 93, 79
—. 1983b, Ap&SS, 95, 425
Kinney, A. L., Schmitt, H. R., Clarke, C. J., Pringle, J. E., Ulvestad, J. S., & Antonucci, R. R. J. 2000, ApJ, 537, 152
Laskar, J. 1990, Icarus, 88, 266
Lauer, T. R., Faber, S. M., Gebhardt, K., Richstone, D., Tremaine, S., Ajhar, E. A., Aller, M. C., Bender, R., Dressler, A., Filippenko, A. V., Green, R., Grillmair, C. J., Ho, L. C., Kormendy, J., Magorrian, J., Pinkney, J., & Siopis, C. 2005, AJ, 129, 2138
Lauer, T. R., Faber, S. M., Groth, E. J., Shaya, E. J., Campbell, B., Code, A., Currie, D. G., Baum, W. A., Ewald, S. P., Hester, J. J., Holtzman, J. A., Kristian, J., Light, R. M., Ligynds, C. R., O'Neil, Jr., E. J., & Westphal, J. A. 1993, AJ, 106, 1436
Lauer, T. R., Faber, S. M., Richstone, D., Gebhardt, K., Tremaine, S., Postman, M., Dressler, A., Aller, M. C., Filippenko, A. V., Green, R., Ho, L. C., Kormendy, J., Magorrian, J., & Pinkney, J. 2007, ApJ, 662, 808
Lauer, T. R., Gebhardt, K., Richstone, D., Tremaine, S., Bender, R., Bower, G., Dressler, A., Faber, S. M., Filippenko, A. V., Green, R., Grillmair, C. J., Ho, L. C., Kormendy, J., Magorrian, J., Pinkney, J., Laine, S., Postman, M., & van der Marel, R. P. 2002, AJ, 124, 1975
Lauer, T. R., Tremaine, S., Ajhar, E. A., Bender, R., Dressler, A., Faber, S. M., Gebhardt, K., Grillmair, C. J., Kormendy, J., & Richstone, D. 1996, ApJ, 471, L79+
Louis, P. D., & Gerhard, O. E. 1988, MNRAS, 233, 337
Lousto, C. O., & Zlochower, Y. 2007, ArXiv e-prints, 708
Madau, P., & Quataert, E. 2004, ApJ, 606, L17
Mediavilla, E., & Arribas, S. 1993, Nature, 365, 420
Mediavilla, E., Guijarro, A., Castillo-Morales, A., Jiménez-Vicente, J., Florido, E., Arribas, S., García-Lorenzo, B., & Battaner, E. 2005, A&A, 433, 79

Merritt, D. 1985, ApJ, 289, 18
—. 2001, ApJ, 556, 245
—. 2006, ApJ, 648, 976
Merritt, D., Berczik, P., & Laun, F. 2007, AJ, 133, 553
Merritt, D., & Ferrarese, L. 2001, MNRAS, 320, L30
Merritt, D., Graham, A. W., Moore, B., Diemand, J., & Terzić, B. 2006a, AJ, 132, 2685
Merritt, D., Milosavljević, M., Favata, M., Hughes, S. A., & Holz, D. E. 2004, ApJ, 607, L9
Merritt, D., Storchi-Bergmann, T., Robinson, A., Batcheldor, D., Axon, D., & Cid Fernandes, R. 2006b, MNRAS, 367, 1746
Miller, R. H. 1996, in Astronomical Society of the Pacific Conference Series, Vol. 102, The Galactic Center, ed. R. Gredel, 327–+
Miller, R. H., & Smith, B. F. 1992, ApJ, 393, 508
Milosavljević, M., & Merritt, D. 2001, ApJ, 563, 34
Milosavljević, M., Merritt, D., Rest, A., & van den Bosch, F. C. 2002, MNRAS, 331, L51
Mineau, P., Feix, M. R., & Rouet, J. L. 1990, A&A, 228, 344
Mulder, W. A. 1983, A&A, 117, 9
Pretorius, F. 2005, Physical Review Letters, 95, 121101
Prugniel, P., & Simien, F. 1997, A&A, 321, 111
Read, J. I., Goerdt, T., Moore, B., Pontzen, A. P., Stadel, J., & Lake, G. 2006, MNRAS, 373, 1451
Redmount, I. H., & Rees, M. J. 1989, Comments on Astrophysics, 14, 165
Rood, H. J., Page, T. L., Kintner, E. C., & King, I. R. 1972, ApJ, 175, 627
Roos, N., Kaastra, J. S., & Hummel, C. A. 1993, ApJ, 409, 130
Schnittman, J. D., & Buonanno, A. 2007, ApJ, 662, L63
Sérsic, J. L. 1963, Boletin de la Asociacion Argentina de Astronomia La Plata Argentina, 6, 41
Sersic, J. L. 1968, Atlas de galaxias australes (Cordoba, Argentina: Observatorio Astronomico, 1968)
Shapiro, S. L. 2005, ApJ, 620, 59
Spinnato, P. F., Fellhauer, M., & Portegies Zwart, S. F. 2003, MNRAS, 344, 22
Sridhar, S. 1989, MNRAS, 238, 1159
Sridhar, S., & Nityananda, R. 1989, Journal of Astrophysics and Astronomy, 10, 279
Szell, A., Merritt, D., & Kevrekidis, I. G. 2005, Physical Review Letters, 95, 081102
Terzić, B., & Graham, A. W. 2005, MNRAS, 362, 197
Tichy, W., & Marronetti, P. 2007, ArXiv General Relativity and Quantum Cosmology e-prints
Tremaine, S. 2005, ApJ, 625, 143
Tremaine, S., & Weinberg, M. D. 1984, MNRAS, 209, 729
Valenzuela, O., & Klypin, A. 2003, MNRAS, 345, 406
Weinberg, M. D. 1989, MNRAS, 239, 549
Weinberg, M. D., & Katz, N. 2002, ApJ, 580, 627
White, M. L. 1949, ApJ, 109, 159
White, S. D. M. 1983, ApJ, 274, 53
Young, P. J. 1977, ApJ, 215, 36
Zaritsky, D., & White, S. D. M. 1988, MNRAS, 235, 289